HAL
open science

MERLIN: A French-German Space Lidar Mission Dedicated to Atmospheric Methane

Gerhard Ehret, Philippe Bousquet, Clémence Pierangelo, Matthias Alpers, Bruno Millet, James Abshire, Heinrich Bovensmann, John Burrows, Frédéric Chevallier, Philippe Ciais, et al.

To cite this version:

Gerhard Ehret, Philippe Bousquet, Clémence Pierangelo, Matthias Alpers, Bruno Millet, et al.. MERLIN: A French-German Space Lidar Mission Dedicated to Atmospheric Methane. Remote Sensing, 2017, 9 (10), pp.1052. 10.3390/rs9101052 . insu-01664230

HAL Id: insu-01664230

https://insu.hal.science/insu-01664230

Submitted on 14 Dec 2017

HAL is a multi-disciplinary open access archive for the deposit and dissemination of scientific research documents, whether they are published or not. The documents may come from teaching and research institutions in France or abroad, or from public or private research centers.

L'archive ouverte pluridisciplinaire **HAL**, est destinée au dépôt et à la diffusion de documents scientifiques de niveau recherche, publiés ou non, émanant des établissements d'enseignement et de recherche français ou étrangers, des laboratoires publics ou privés.

remote sensing

MDPI

Review

MERLIN: A French-German Space Lidar Mission Dedicated to Atmospheric Methane

Gerhard Ehret [1,*], Philippe Bousquet [2], Clémence Pierangelo [3], Matthias Alpers [4], Bruno Millet [3], James B. Abshire [5], Heinrich Bovensmann [6], John P. Burrows [6], Frédéric Chevallier [2], Philippe Ciais [2], Cyril Crevoisier [7], Andreas Fix [1], Pierre Flamant [7,8], Christian Frankenberg [9], Fabien Gibert [7], Birgit Heim [10], Martin Heimann [11,12], Sander Houweling [13,14], Hans W. Hubberten [10], Patrick Jöckel [1], Kathy Law [8], Alexander Löw [15,†], Julia Marshall [11], Anna Agusti-Panareda [16], Sebastien Payan [8], Catherine Prigent [17], Patrick Rairoux [18], Torsten Sachs [19], Marko Scholze [20] and Martin Wirth [1]

1 Deutsches Zentrum für Luft- und Raumfahrt (DLR) Oberpfaffenhofen, Institut für Physik der Atmosphäre, 82234 Weßling, Germany; Andreas.Fix@dlr.de (A.F.); Patrick.Joeckel@dlr.de (P.J.); Martin.Wirth@dlr.de (M.W.)
2 Laboratoire des Sciences du Climat et de l'Environnement (LSCE), LSCE-IPSL (CEA-CNRS-UVSQ), IPSL, 91191 Gif sur Yvette, France; Philippe.Bousquet@lsce.ipsl.fr (P.B.); Frederic.Chevallier@lsce.ipsl.fr (F.C.); Philippe.Ciais@lsce.ipsl.fr (P.C.)
3 Centre National D'Etudes Spatiales(CNES), 31400 Toulouse, France; Clemence.Pierangelo@cnes.fr (C.P.); Bruno.Millet@cnes.fr (B.M.)
4 Deutsches Zentrum für Luft- und Raumfahrt, Raumfahrtmanagement (DLR), 53227 Bonn, Germany; Matthias.Alpers@dlr.de
5 NASA Goddard Space Flight Center (GSFC), Greenbelt, MD 20771, USA; James.B.Abshire@nasa.gov
6 Institute of Environmental Physics, University of Bremen, 28359 Bremen, Germany; Heinrich.Bovensmann@uni-bremen.de (H.B.); Burrows@iup.physik.uni-bremen.de (J.P.B.)
7 Laboratoire de Météorologie Dynamique (LMD), Ecole Polytechnique, 91128 Palaiseau, France; Cyril.Crevoisier@lmd.polytechnique.fr (C.C.); Pierre.Flamant@latmos.ipsl.fr (P.F.); Gibert@lmd.polytechnique.fr (F.G.)
8 Laboratoire Atmosphères, Milieux, Observations Spatiales (LATMOS), IPSL, CNRS-UVSQ-UPMC, 75005 Paris, France; Kathy.Law@latmos.ipsl.fr (K.L.); Sebastien.Payan@latmos.ipsl.fr (S.P.)
9 NASA Jet Propulsion Laboratory (JPL), Pasadena, CA 91109, USA; Christian.Frankenberg@jpl.nasa.gov
10 Alfred-Wegener-Institut (AWI), Helmholtz -Zentrum für Polar- und Meeresforschung, Telegrafenberg, 14473 Potsdam, Germany; Birgit.Heim@awi.de (B.H.); Hans-Wolfgang.Hubberten@awi.de (H.W.H.)
11 Max-Planck-Institut (MPI) für Biogeochemie, 07745 Jena, Germany; Martin.Heimann@bgc-jena.mpg.de (M.H.); Marshall@bgc-jena.mpg.de (J.M.)
12 Division of Atmospheric Sciences, Department of Physics, University of Helsinki, 00100 Helsinki, Finland
13 SRON Netherlands Institute for Space Research Utrecht, 3584 CA Utrecht; The Netherlands, S.Houweling@sron.nl
14 Department of Earth Sciences, Vrije Universiteit, 1081 HV Amsterdam, The Netherlands
15 Faculty of Geosciences, Department of Geography, Ludwig-Maximilians-Universität (LMU), 80539 München, Germany
16 European Centre for Medium-Range Weather Forecasts (ECMWF), Reading RG2 9AX, UK; Anna.Agusti-Panareda@ecmwf.int
17 Centre National de la Recherche Scientifique (CNRS), Observatoire de Paris, 75016 Paris, France; Catherine.Prigent@obspm.fr
18 Institut Lumière Matière, UMR5306 Université Lyon 1-CNRS, Université de Lyon, 69622 Villeurbanne, France; Patrick.Rairoux@univ-lyon1.fr
19 Helmholtz-Zentrum Potsdam—Deutsches GeoForschungsZentrum (GFZ), Telegrafenberg, 14473 Potsdam, Germany; Torsten.Sachs@gfz-potsdam.de
20 Department of Physical Geography and Ecosystem Science, Lund University Box 117, 221 00 Lund, Sweden; Marko.Scholze@nateko.lu.se
* Correspondence: Gerhard.Ehret@dlr.de; Tel.: +49-8153-28-2509
† Deceased.

Received: 26 August 2017; Accepted: 2 October 2017; Published: 16 October 2017

Abstract: The MEthane Remote sensing Lidar missioN (MERLIN) aims at demonstrating the spaceborne active measurement of atmospheric methane, a potent greenhouse gas, based on an Integrated Path Differential Absorption (IPDA) nadir-viewing LIght Detecting and Ranging (Lidar) instrument. MERLIN is a joint French and German space mission, with a launch currently scheduled for the timeframe 2021/22. The German Space Agency (DLR) is responsible for the payload, while the platform (MYRIADE Evolutions product line) is developed by the French Space Agency (CNES). The main scientific objective of MERLIN is the delivery of weighted atmospheric columns of methane dry-air mole fractions for all latitudes throughout the year with systematic errors small enough (<3.7 ppb) to significantly improve our knowledge of methane sources from global to regional scales, with emphasis on poorly accessible regions in the tropics and at high latitudes. This paper presents the MERLIN objectives, describes the methodology and the main characteristics of the payload and of the platform, and proposes a first assessment of the error budget and its translation into expected uncertainty reduction of methane surface emissions.

Keywords: MERLIN; space mission; IPDA Lidar; atmospheric methane; CH_4 emissions; global methane budget

1. Introduction

Monitoring methane (CH_4) atmospheric concentrations from space is an important but challenging scientific problem.

It is important because human-induced emissions and land use changes make the global concentration of CH_4 increase and contribute to additional radiative forcing with other increasing greenhouse gases, ultimately leading to the rise of the global mean Earth surface temperature [1]. Methane emissions have various sources, mostly anthropogenic (~2/3), which can be grouped around three processes [2]: the biogenic anaerobic degradation of organic matter by archaea (natural wetlands and inland waters, enteric fermentation and manure, rice cultivation, waste management, termites); the thermogenic formation in the Earth's crust under high temperatures and pressure (natural degassing of the Earth's crust, exploitation of fossil fuels); and the pyrogenic combustion of biomass under low-O_2 condition (biomass and biofuel burning). Even if total methane emissions are estimated with a global uncertainty of only 5–6% by atmospheric-based studies, this uncertainty increases to 20–30% for process-based estimates, and individual sources have uncertainties on the order of 30–40% for anthropogenic sources and larger than 100% for some natural sources (e.g., freshwater emissions, e.g., [2]).

Methane dry-air mole fractions have been directly measured with high accuracy (better than 0.1% in the last years, [3]) at reference ground-based stations since the late 1970s [4]. The surface networks have developed throughout the years and, today, provide more than 150 regularly sampled or continuous point measurements at the surface or along tall towers [3]. They are complemented by regular vertical profiles and transects by small airplanes in the planetary boundary layer (e.g., [5]) or by commercial aircraft [6,7] and by some regional aircraft campaigns (e.g., [8–10]). The concept of AirCore [11] has also offered the possibility to measure vertical profiles of greenhouse gases (GHG) from the surface to the stratosphere (up to 30 km). On the remote-sensing side, the Total Carbon Column Observing Network (TCCON) uses ground-based Fourier transform spectrometers (FTS) to measure atmospheric column abundances of CH_4 and other molecules using solar absorption spectroscopy in the near-infrared spectral region [12]. This surface-based remote-sensing technique makes use of sunlight, and can only be performed throughout the day during clear sky conditions, with the sun typically at least 10° above the horizon. During the last years solar absorption spectrometry, using backscattered sunlight detected with a spectrometer on an aircraft [13], was used to estimate CH_4

emissions from strong and localized point sources like coal mine [14] ventilation shafts, or landfills [15], for instance.

Surface-based CH_4 observations have been used for decades to estimate CH_4 sources using data-driven methods and atmospheric inversion techniques, which optimally combine observed mole fractions ratios, some prior knowledge about emissions and sinks, and an atmospheric transport and chemistry model linking emissions and sinks to atmospheric observations (e.g., [2,16,17]). Converting atmospheric observations to surface emissions has been done mostly from global scale to regional scale (e.g., [2]). However, recently, various multi-institution collaborations have developed methodologies for the quantification of methane emissions in urban environments such as in Indianapolis (Indiana) or Los Angeles (California) in the United States (e.g., [18–21]). The importance of the monitoring of GHG surface fluxes based on atmospheric observations has grown in the context of climate change mitigation after the Paris climate agreement, because it in principle allows emissions and their changes to be tracked with independent data from country-based declarations to the United Nations Framework Convention on Climate Change (UNFCCC).

The inversion systems inferring CH_4 emissions from CH_4 mole fractions are limited by the quality of the underlying atmospheric transport model used (e.g., [22,23]) and by the uneven distribution of surface observations in space and time (e.g., [24]). Some key regions for the biogeochemical cycles of GHGs remain extremely difficult to access for long-term scientific activities because of their remote location or their political situation (e.g., the Arctic, tropical forests, some African countries). In addition, industrialized regions often have many different sources of CH_4 from, for example, livestock, fuel extraction and waste—some of them concentrated in hotspot regions—which requires high spatial density surface networks to separate and quantify those sources individually [25].

In this context, measuring CH_4 from space becomes important, as it offers a drastic improvement in observational capacity to potentially provide either global coverage of CH_4 concentrations on a regular temporal basis (solar synchronous orbits), or regional coverage with continuous observations during daytime (geostationary orbits).

However, the monitoring of a trace gas such as CH_4 from space at a sufficient precision and accuracy to determine the changes in the plume resulting from changes in surface emissions is challenging. This is because the magnitude and variability of the absorption signal measurable at the top of the atmosphere for atmospherically relatively long-lived gases such as CH_4 is relatively small in comparison to the changes in reactive gases such as O_3 and CO, for example. Further, the accurate retrieval of these small changes is limited by the knowledge of spectroscopic parameters and of other atmospheric species which may have overlapping absorptions in the same spectral region. Recent progress in the methane spectroscopy in the near-infrared should reduce uncertainty in retrievals (e.g., [26]). CH_4 fluxes emitted from the surface result in small changes in the spatial distributions of the above CH_4 dry column mole fraction (e.g., typically a few ppb, and up to a few tens of ppb, on a day-to-day basis and at a typical model spatial resolution of 200 $\times$ 200 km, (see Science Plan of MEthane Remote sensing Lidar missioN (MERLIN) [27] with most of the variation happening in the boundary layer. The level of measurement uncertainty that is required in this context to identify such changes above atmospheric background (~1800 ppb) is typically lower than $\pm$2% for the total measurement error, with low systematic errors. Such an already ambitious objective for a space-based measurement of methane columns is still far from the recommendation of the World Meteorological Organisation (WMO) for surface in situ observations of atmospheric methane, which is to be better than $\pm$2 ppb (<0.1%, for point in situ measurements [28]).

In the decade beginning in 2000, two passive instruments were launched into sun synchronous orbits and have provided column-averaged dry air mole fractions (XCH_4) using shortwave infrared absorption spectrometry (SWIR). Between 2002 and 2012, the Scanning Imaging Absorption spectrometer for Atmospheric CHartographY (SCIAMACHY) was operated on board ESA's (European Space Agency) ENVIronmental SATellite [29–34]. In January 2009, the JAXA (Japan Aerospace Exploration Agency) satellite Greenhouse Gases Observing SATellite (GOSAT) was

launched with the TANSO-FTS instrument [35,36]. Global and regional inverse modelling of CH_4 fluxes made use of SCIAMACHY [37–41] and GOSAT [22,42,43] satellite retrievals to infer CH_4 emissions. Passive SWIR instruments offer a limited coverage in cloud-covered regions and in high latitudes from the autumn to the spring equinox. Instruments based on thermal infrared (TIR) spectroscopy can retrieve XCH_4 at high latitudes, but are much more sensitive to mid-troposphere concentrations than to concentrations in the boundary layer where CH_4 emissions occur. Recently, CH_4 data from SCIAMACHY and GOSAT was also used to detect and quantify local emission hotspots from oil/gas production and coal mining (e.g., [44,45]). Although it offers very low sensitivity in the boundary layer, data from Infrared Atmospheric Sounding Interferometer (IASI) flying on the European MetOp satellite series since 2006 [46] also provides statistically consistent methane emissions [42].

Passive satellite data have brought a new vision of the space-time distribution of CH_4 atmospheric mole fractions that complements that from the surface observations, albeit with comparatively lower precision and accuracy. The use of SCIAMACHY to infer CH_4 emissions in global inversions necessitates the use of accurate radiative transfer models in the retrieval of XCH_4, which account for scattering by cirrus and aerosol. As a result of the loss of a SCIAMACHY detector at the end of 2005, instrumental noise increased, resulting in XCH_4 retrieval uncertainties increasing up to 40 ppb [38,40,47]. Although GOSAT retrievals still present significant biases [31,48], these data represent an important improvement both for random and residual systematic errors, the latter being now estimated to be only 4–6 ppb on individual column soundings [48].

Several passive missions aiming to measure CH_4 (Table 1) are scheduled to be launched in the upcoming years. TROPOMI on ESA Sentinel 5 Precursor is planned to be launched in 2017 [49], followed by JAXA-NIES-MOE GOSAT-2 in 2018 [50]. NASA plans the geostationary mission geoCARB [51] to be launched after 2020, while CNES and EUMETSAT are preparing the next generation of IASI (IASI-NG, 2021) [52] and ESA-EUMETSAT are preparing UVNS/Sentinel 5 (2021). In this context of the evolving development of passive instruments, the MEthane Lidar missioN (MERLIN) proposes an active measurement of XCH_4 by employing an IPDA (Integrated Path Differential Absorption) nadir-viewing Lidar instrument [53–56]. As described below, this new technique has the potential to deliver global coverage during all seasons and with low systematic errors. In view of this potential benefit, the development of Lidar sensors for the measurement of CH_4, and also CO_2, has attracted increasing attention. Several experimental setups have been tested by different groups, each using slightly different approaches [57–63]. Recent efforts in the framework of NASA's ASCENDS (Active Sensing of CO_2 Emissions over Nights, Days, and Seasons) mission proposal have led to a significant step towards an active CO_2 sensor in space (NASA report on ASCENDS, and references therein [64]). For CH_4, reports on active airborne measurements are still sparse [65]. CHARM-F, DLR's new airborne IPDA Lidar instrument for CH_4 and CO_2, has just recently been completed and tested on the German research aircraft HALO (High Altitude and Long Range Research Aircraft) for the first time [66]. Initial results from this campaign show a high measurement precision (<0.5%) for both species, even in strongly varying geophysical conditions (mountain-like topography, surface albedo jumps, water surfaces, atmospheric aerosol load, and cloudy conditions).

MERLIN is a joint French (CNES) and German (DLR) space mission, with a launch scheduled for the timeframe 2021/22 (Table 1). The development of the payload is the responsibility of the German space agency (DLR), while the platform (MYRIADE Evolutions product line) is that of the French space agency (CNES). The IPDA technique foreseen for MERLIN relies on DIAL (Differential Absorption Lidar) measurements using a pulsed laser emitting at two frequencies around a methane line multiplet at 1.64 μm. One wavelength is accurately locked to a spectral feature of the CH_4 absorption manifold, minimizing any small frequency shifts, to diminish potential systematic errors. The other frequency is selected to have negligible CH_4 absorption and is used as the reference. The MERLIN instrument concept, the measurement approach, and frequency selection are similar to the CHARM-F instrument, mentioned above. An Optical Parametric Oscillator (OPO) pumped by a Nd:YAG laser will serve as the MERLIN transmitter to make use of DLR's long-term experience with such devices for atmospheric

water vapor profiling [67]. With respect to space application, this technical concept will benefit from ESA's laser development program in connection to the Earth Explorer Aeolus (ALADIN) and EarthCARE (ATLID) [68]. Further heritage on the instrument readiness level is provided by the NASA/CNES CALIPSO mission that uses high average power Nd:YAG lasers as Lidar transmitters in space over a period of more than 10 years [69,70]. To mitigate the risk of the spaceborne pump laser development for MERLIN, the conceptual design will make use of the so-called "Future Laser System" FULAS development, which is a cooperation between ESA and DLR to advance spaceborne laser technology [71].

This active method does not require reflected sunlight, and enables measurements to be made in all seasons at all latitudes, during daylight and night. The differential approach, the size of the laser spot (~120 m at the surface along the track), and the selective sampling guarantees low systematic errors (target < 3.7 ppb) and measurements in broken cloud condition, with almost no contamination by aerosol or water vapor. MERLIN observations promise to enhance the effective constraints brought by satellite data on methane surface emissions once assimilated into atmospheric modelling systems. Given the experience in the development and operation of previous Lidar missions in space, a mission lifetime of three years for MERLIN appears feasible.

In this manuscript, the MERLIN mission objectives (Section 2), the methodology employed (Section 3), the different mission elements (Section 4), a first analysis of the expected performances (Section 5), and conclusions are presented.

Table 1. Comparison of MEthane Remote sensing Lidar missioN (MERLIN) mission with other past, current, decided, or proposed missions measuring methane with characteristics that are suitable for source estimation.

Parameter/Information	MERLIN	SCIAMACHY	GOSAT	GOSAT-2	Sentinel 5P TROPOMI	Sentinel 5	IASI	geoCARB	IASI-NG
Agencies	DLR/CNES	DLR/NSO/ESA	JAXA	JAXA	ESA/NSO	ESA	CNES/EUMETSAT	NASA	CNES/EUMETSAT
Orbit	Low sun synchronous	Low sun synchronous	Low sun synchronous	Low sun synchronous	Low sun synchronous	Low sun synchronous	Low sun synchronous	Geo-stationary	Low sun synchronous
Meas. tech.	Active Lidar	Passive SWIR	Passive SWIR	Passive SWIR	Passive SWIR	Passive SWIR	Passive TIR	Passive SWIR	Passive TIR
Mission status	Selected and funded	Terminated 2012	In orbit and functioning	Selected and funded	Selected and funded	Selected and funded	Selected and funded	Selected and funded	Selected and funded
Spectr. window (μm) [a]	1.64555/ 1.64585 [b]	1.63–1.70 2.23–2.34	1.63–1.70	1.63–1.70 2.33–2.38	2.31–2.39	1.63–1.70 2.31–2.39	3.62–15.50	2.3–2.34	3.62–15.50
Launch date	2021/22	2002	2009	2018	2017	2022	2006/13/18 MetopA/B/C)	2022/23	2021/28/35 (Metop-SG-A1/A2/A3)
Product	XCH_4	XCH_4, XCO_2, SIF, other react. gases	XCH_4, XCO_2, SIF	XCH_4, XCO_2, XCO, SIF	XCH_4, SIF, other react. gases	XCH_4, SIF, other react.gases	Free trop. XCH_4 and others	XCH_4, XCO_2, other react. gases	Free trop. XCH_4 and others
Revisiting time (days)	28	6	3	6	1	1	1	2–8 h [c]	1
Smallest spot size (km^2)	0.15 × 0.15	30 × 60	Circular 10 km diam.	Circular 10 km diam.	7 × 7	7 × 7	12 × 12	4 × 5 [d]	12 × 12
Soundings/s	20	3	0.25	0.25	215	215	215	~250	215
Overpass time (local)	06:00/18:00	10:00	13:00	13:00	13:30	9:30	09:30/21:30	Continuous during daylight	09:30/21:30
References	This paper	[32,72]	[73]	[50]	[74]	[75]	[46]	[76]	[52]

[a] Only windows for CH_4 detection are listed; [b] Online/offline wavelengths; [c] At continental scale; [d] Resolution at roughly 30°. The resolution is degraded when latitude increases. German Space Agency (DLR); French Space Agency (CNES); SCanning Imaging Absorption spectroMeter for Atmospheric CHartographY (SCIAMACHY); Greenhouse Gases Observing SATellite (GOSAT); shortwave infrared absorption spectrometry (SWIR); Netherlands Space Office (NSO); European Space Agency (ESA); Japan Aerospace Exploration Agency (JAXA); thermal infrared (TIR); Tropospheric Monitoring Instrument (TROPOMI); solar-induced chlorophyll fluorescence (SIF); National Aeronautics and Space Administration (NASA); European Organisation for the Exploitation of Meteorological Satellites (EUMETSAT); geostationary carbon cycle observatory (geoCARB); new generation of infrared atmopsheric sounding interferometer (IASI-NG).

2. Mission Objectives

The overarching scientific goal of the French-German Climate Mission MERLIN is to provide atmospheric constraints to improve our knowledge of the global methane emissions and sinks. This scientific goal is to be achieved by the development, launch and operation of an Earth observation satellite in the framework of a French-German cooperation. The mission aims to provide information on the global methane cycle at all latitudes, including the still-underexplored regions such as tropical lands and high latitudes. The measurements are consequently of relevance for climate change research, and with respect to the monitoring approach needed for the implementation of the Paris Climate Agreement signed during COP21 in December 2015. Indeed, CH_4 is a potent greenhouse gas, and has interesting mitigation options due to its limited lifetime of approximately nine years [77] which is shorter than that of most other anthropogenic greenhouse gases, thus offering a variety of mitigation opportunities in different sectors (e.g., [2,78,79]). It is therefore important to measure its atmospheric variations with time and to develop methods to estimate its sources and sinks independently from the Intended National Determined Contributions (INDCs) provided by the signatory countries.

The main scientific objective of MERLIN is to deliver column-weighted dry-air mole fractions of CH_4, referred to as XCH_4 along the satellite sub-track with a targeted random error better than 27 ppb (Table 3, 50 km averaging along the satellite track, as illustrated in Figure 1) and a systematic error better than 3.7 ppb (68% interval). As a novel feature, the MERLIN mission will use pulsed narrow-bandwidth laser radiation, thus not relying on sunlight or Earth infrared emission. With a range-gated receiver for detection of the signals reflected from the Earth's surface or from optically thick clouds, the MERLIN instrument will distinguish surface from cloud or aerosol backscatter, permitting high-precision retrievals of XCH_4 in the presence of particle layers with low optical depth, such as thin cirrus or aerosol. In the presence of optically thick clouds, the Lidar beam can reach the surface when gaps between clouds occur due to the near-nadir view and the small Lidar ground spot. MERLIN can also provide XCH_4 measurements above dense stratiform clouds to be used as a reflective target instead of the surface target. As MERLIN has its own transmitter, its observations will produce data at high latitudes, in winter and at night. MERLIN XCH_4 will complement and enhance the existing observation systems for GHG monitoring, complementing surface-based, balloon, aircraft and passive satellite observations. In addition to XCH_4, the MERLIN products will also include information on secondary climate-relevant parameters, for example, cloud top heights, surface retro-reflectance and, potentially, canopy height. MERLIN XCH_4 will nicely complement existing measurement techniques by providing XCH_4 where either surface networks (tropics, high latitudes) or other satellites (high latitude winter, night, some cloudiness conditions) provide no or only sparse observations in space and time.

MERLIN will deliver maps of XCH_4, built from XCH_4 measurements using an original Bayesian approach [80] that provides daily global maps of XCH_4 with reliable (in the statistical sense) associated uncertainties in the form of a full space-time covariance matrix. These maps will be used, together with their error statistics, to rigorously compare the retrievals with distant validation data, in the absence of a target mode for MERLIN.

The main scientific goal of the MERLIN mission is to contribute to the estimations of CH_4 sources and sinks using atmospheric inversions in order to reduce uncertainties in the global CH_4 cycle. Indeed, MERLIN should provide insights for the different scientific communities working on CH_4 sources and sinks including activities around land-surface modelling, emission inventories, and atmospheric chemistry. With a revisit time of 28 days and the ability to measure at all seasons, MERLIN will help constrain surface sources and sinks from seasonal (e.g., changes in gas leaks from winter to summer) to annual scale (e.g., evolution of regional sources during the three years of the mission). The inverse modelling used to convert the atmospheric columns into source estimates is not formally part of the MERLIN mission scope handled by space agencies. Uncertainties in the estimates of CH_4 sources and sinks from XCH_4 products suggest that several modelling groups should develop their own approaches, as was done for previous GHG missions. Ensemble atmospheric inversions have

proven to be more robust than individual studies to represent the remaining uncertainties in the global methane cycle (e.g., [27]) Hence, by providing global and low-biased XCH_4 data, MERLIN will help reducing uncertainties both in the global and regional methane cycle (Section 5).

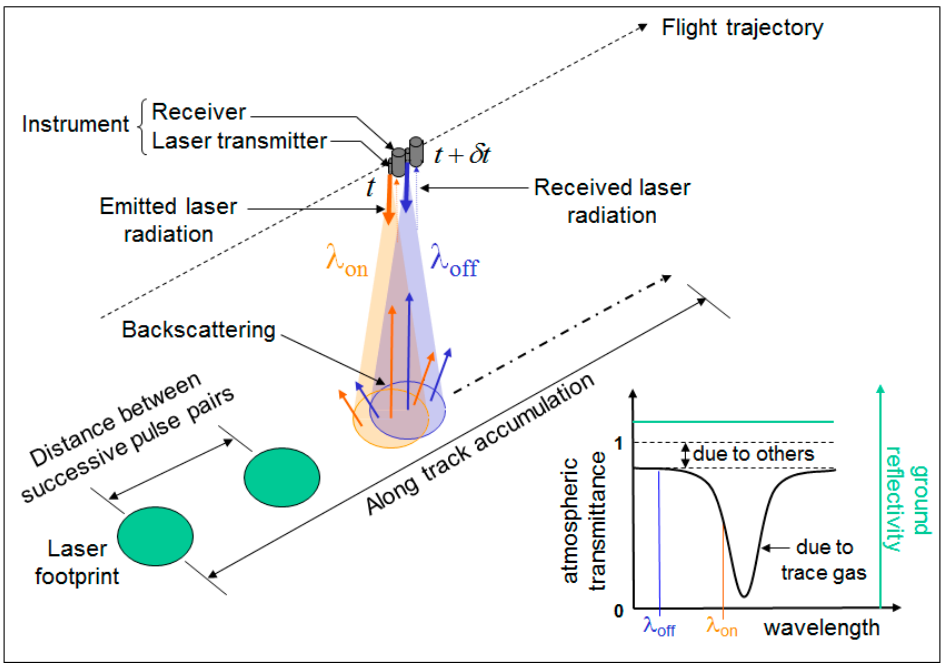

Figure 1. Schematic diagram of a two-frequency Integrated Path Differential Absorption (IPDA) Lidar measurement. It makes use of the small fraction of emitted laser radiation which is reflected by a "hard" target (i.e., the Earth's surface or a cloud top) towards the instrument's receiver, and subsequently converted into electrical signals by a photodetector. Both signals from online and offline pulses are digitized and corrected for the energy of the emitted laser pulses which are monitored within the instrument. Many such pulse-pairs are accumulated along the instrument's ground track to increase the measurement precision. The ground reflectivity and beam attenuation from contributors other than the trace gas are typically constant at the very narrow spectral scale of a molecular absorption line, as shown using dashed lines in the right-hand corner.

One further objective of the MERLIN mission is to deliver XCH_4 retrievals to operational centers such as the Copernicus Atmosphere Monitoring Service [81] at the European Centre for Medium range Weather Forecasts (ECMWF), which assimilates satellite GHG observations to initialize its GHG forecasts [82]. Following this objective, the MERLIN mission plans to deliver these products within two days of acquisition, as it is currently implemented for the GOSAT data used within CAMS.

MERLIN will also be a scientific and technological demonstrator. On the scientific side, if XCH_4 has the expected performances in terms of systematic errors, MERLIN will provide the first very low-biased space-based GHG data. Such low-biased data will be highly useful to the scientific community, especially for atmospheric inversions. This will in turn facilitate the evolution of verification systems to test the GHG emissions reported at the country level, that is, independent data complementary to the country declarations to the UNFCCC based on inventories. Until now, only country-based declarations from inventories have been used to officially report GHG emissions. In the case of CH_4, inventories are associated with large errors because those emissions are often fugitive, related more to processes controlling emissions than to a measurable feedstock or pool. Atmospheric inversions can provide a complementary approach. This is especially true for changes (inter-annual variations, trends, etc.) in regional to global emissions, which can generally be more safely inferred than total annual emissions because (at least) some systematic errors vanish when

looking at the difference between two time periods (e.g., [16,83]). The success of MERLIN would open the possibility to develop, jointly with surface observations and passive missions providing CH_4 imagery, inversion frameworks for the monitoring of regional CH_4 emission changes with time. Such an alternative to country declarations is critical for the success of the implementation of the Paris Climate Agreement. On the technological side, the success of a Lidar mission for greenhouse gases on a microsatellite would open a path to further Lidar system developments. By offering campaign possibilities, the validation phase of MERLIN is the occasion to stimulate research and test new technologies, including ground-based or aircraft-based remotesensing approaches and to prepare future active GHG missions.

3. Methodology

As a novel feature, MERLIN will make use of the IPDA Lidar technique to derive XCH_4. The envisaged methodology and basic measurement concept has been developed in the framework of two dedicated ESA studies [84,85] to support the Advanced Space Carbon and Climate Observation of Planet Earth (A-SCOPE) study for CO_2 [86], and subsequent studies focusing on CH_4 [55,87]. The Lidar instrument measures the reflected or scattered radiation from the Earth's surface and from cloud tops along the satellite footprint as depicted schematically in Figure 1. For each measurement, the ground spot will be illuminated by spectrally narrow laser pulses having slightly different frequencies in the 1.64 µm spectral domain, commonly denoted as online and offline frequencies, respectively. To be sensitive to the CH_4 concentration changes close to the Earth's surface, the online frequency will be accurately positioned on the wing of a pressure-broadened CH_4 absorption line. In contrast, selection of a frequency position on the CH_4 absorption line center would give highest sensitivity in the stratosphere. In general, the absorption feature of spectrally narrow laser radiation is determined by the Weighting Function (WF), which in principle describes the relative contribution of an atmospheric layer at pressure p to XCH_4 (see Figures 1 and 2 in [53] and Equation (3)). The spectral precision is possible since the spectral width of the laser pulses is set by the constructor at about 60 MHz (FWHM). Hence, it can be regarded as being quasi-monochromatic compared to the pressure-broadened CH_4 absorption line of about 3 GHz (FWHM). As in usual laser differential-absorption methodology, each online measurement is accompanied by corresponding offline measurement that serves as a reference exhibiting significantly less CH_4 absorption. Both online and offline frequencies are sequentially emitted with a very short time delay ($\Delta t \sim 250$ µs) in order to observe near-identical light paths and surface scattering properties.

The signals received by the payload can be described using the hard target Lidar equation [53]:

$$P_{on,off}(r_T) = D_{on,off}\frac{A}{r_T^2}O_{on,off}\rho_{on,off}\tau^2_{on,off}(r_T)\frac{E_{on,off}}{\Delta t_{eff}} \tag{1}$$

For both frequencies, P is the instantaneous light power entering the detector area from reflecting target at range r_T, D is the total optical efficiency, A is the size of the telescope area, O the overlap function between laser ground spot and the field of view (FOV) of the receiving telescope at the target, ρ [sr^{-1}] is the target reflectance parameter defined as the reflected power towards the receiver divided by the incident power, $\tau_{on,off}$ is the one-way atmospheric transmission, $E_{on,off}$ are the emitted pulse energies at both frequencies which slightly differ in real lasers systems, and Δt_{eff} is the effective pulse length, given by the time spread of the structured target, the temporal length of the emitted pulses, and the detector impulse response time. By applying the Beer-Lambert law, the Differential Atmospheric Optical Depth (DAOD) with respect to CH_4 is given by the ratio P_{off}/P_{on} of the measured Lidar signals:

$$\begin{aligned} DAOD(r_T) &\equiv \int_{TOA}^{r_T} m_{CH_4}(r')[1-q_{H_2O}(r')]n_{air}(r')[(\sigma_{on}(r')-\sigma_{off}(r')]dr' \\ &= \tfrac{1}{2}\ln\left[\tfrac{P_{off}(r_T)E_{on}}{P_{on}(r_T)E_{off}}\right] - DAOD_{other\ gases} \end{aligned} \tag{2}$$

In this equation, m_{CH4} is the dry-air mixing ratio of CH_4 at a given distance r', q_{H2O} is the water vapor mixing ratio, n_{air} is the number density of air, and $\sigma_{on,off}$ denotes the respective molecular absorption cross sections for the selected online and offline frequencies. The integration runs from top of the atmosphere (TOA) down to the target distance r_T. On the right-hand side of Equation (2) a further term appears that sums all other DAOD contributions from interfering gases, notably H_2O and CO_2. In principle, the contribution of these spectroscopic terms can be minimized by a careful selection of the quasi-monochromatic laser frequency position within a chosen CH_4 absorption band, which should be almost free from interfering gases. As a unique side effect of our approach, investigations revealed that the water vapour interference can be significantly further reduced by applying the so-called water vapor compensation mode [55,88]. It is based on the idea of choosing the offline position within a water vapour line such that a measurable water vapor $DAOD_{H2O}$ appears, which then partly compensates the water vapour contribution related to the dry-air mixing ratio calculation (left hand side of Equation (2)). It is worth mentioning that the scattering and extinction properties of the atmosphere can be regarded to be identical for both frequencies and will not contribute to a measurement bias, which is a key asset of the proposed measurement principle. A further advantage of using pulsed lasers relates to the known light path, which is indisputably defined by the viewing geometry of the Lidar instrument and the round-trip time of the transmitted laser pulses with typical pulse lengths of a few tens of nanoseconds. However, small amounts of multiple scattering from penetration of optically thick aerosol layers and optical thin cirrus clouds could impact on the length of the light path, and thus can give rise to a measurement error. This impact will be suppressed by choosing a narrow transmitter divergence in conjunction with a narrow receiver field of view.

For modelling purposes it is convenient to introduce pressure coordinates using the hydrostatic equation in combination with the ideal gas law. By this convention, the column-integrated dry-air mixing ratio of CH_4 can be calculated from measured DAOD using the following identity:

$$XCH_4 \equiv \frac{\int_0^{p_T} m_r(p)WF(p)dP}{\int_0^{p_T} WF(p)dp} = \frac{DAOD}{\int_0^{p_T} WF(p,T)dp} = \frac{\ln\left[\frac{P_{off}(r_T)E_{on}}{P_{on}(r_T)E_{off}}\right] - DAOD_{other\ gases}}{2\int_0^{p_T} WF(p,T)dp} \quad (3)$$

where

$$WF(p) = \frac{\sigma_{on}(p,T) - \sigma_{off}(p,T)}{g(p)M_{air}(1 + M_{H_2O}q(p)_{dry})}$$

denotes the weighting function. This function contains the differential absorption cross section for methane, given as function of pressure and temperature, g is the acceleration of gravity, M_{air} and M_{H2O} are the masses of dry air and water vapour molecules, and q_{dry} is the water vapour mixing ratio with respect to dry air. Information of the observed air mass is obtained from the integration of WF, spanning the column between pressure 0 at TOA and p_T the pressure at the location of the target (e.g., laser footprint on the target). Note that to obtain this information by passive remote sensing, an additional oxygen channel is required. If the target is the Earth's surface, p_T will be the surface pressure p_{surf}. It will be derived using operational analyzes from Numerical Weather Prediction (NWP) centres, after correction for a pressure change given by the target height, commonly denoted Surface Scattering Elevation (SSE), as shown in the conceptual drawing of Figure 2.

The elevation correction can be calculated assuming hydrostatic equilibrium:

$$p_{surf} = p_{NWP} \exp\left[\frac{SSE - Z_{NWP}}{-R \cdot T_{NWP}(p)} g\right] \quad (4)$$

where $T_{NWP}(p)$, p_{NWP}, and Z_{NWP} are the modelled vertical temperature profile, surface pressure and the surface elevation of the NWP analyses for the grid box in which the measurement is located. R denotes the gas constant for air. SSE is an ancillary data product that results from knowledge of the orbit height, instrument pointing, and measurement of the distance to the target (r_T) given by

laser ranging methods. The geophysical auxiliary parameters (surface pressure, temperature profiles and water vapour profiles) are provided by (NWP) centres. Absorption cross sections of methane and other "interfering gases" for the desired temperature and pressure ranges are derived from line-by-line calculations using updated spectroscopic databases in combination with numerical models for the calculation of the integrated weighting function [26]. This method can also be applied to infer additional information on partial CH_4 columns above cloudy scenes by taking the signal reflected (scattered) by cloud particles at cloud tops [66]. In that case, p_T will be the pressure at cloud top height and SSE corresponds to the height of the cloud top above Z_{NWP}.

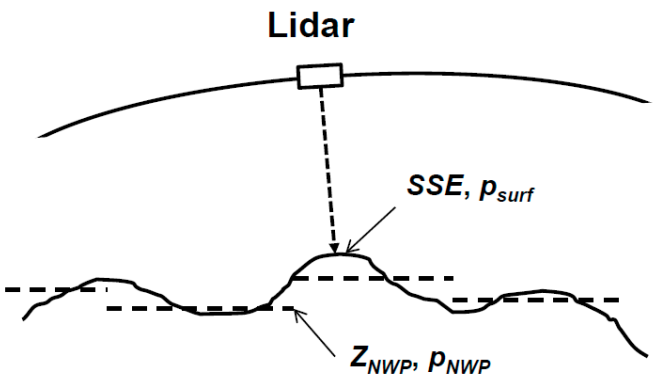

Figure 2. Conceptual drawing illustrating on the definition of Surface Scattering Elevation (SSE) and local surface pressure p_{surf} according to the description in Section 3.

4. Mission Elements

The MERLIN mission concept as detailed in Section 3 is driven by the need to fulfil the scientific objectives and requirements for accurately measuring XCH_4, as discussed in Section 2. Besides the satellite, other mission elements such as the orbit, data processing and validation will have a strong impact on the quality of the products. These mission elements are described in the following.

4.1. Space Segment

The space segment of MERLIN is comprised of a mini-class satellite carrying only one scientific instrument, an IPDA Lidar system operating in a near-nadir-viewing configuration (Figure 3). To share the philosophy of a joint development between France and Germany, the satellite uses a modular approach with a clear separation between the payload provided by Germany (DLR) and the platform module from France (CNES). Figure 4 illustrates the assembled Lidar instrument with its various subsystems attached. All optical units (laser head, telescope, star tracker) are mounted on a common stiff optical bench with an isostatic interface to the spacecraft panel. Other subsystems, such as the Instrument Control Unit (ICU), Frequency Reference Unit (FRU), and Laser Electronics Unit (LEU), will be hard-mounted on a secondary structure, which also contains a thermal interface to a radiator not shown in this figure. The online and offline pulses in the 1.64 µm spectral domain are generated by the laser head (Figure 4b) consisting of an OPO that is pumped by a pulsed single-frequency Nd:YAG laser at 1.064 µm. By means of injection seeding using a continuous wave (cw) single-frequency laser system at 1.64 µm, the OPO provides itself spectrally narrow pulses which can be tuned to the desired frequency position within the absorption profile of the selected molecular transition. The spectral properties of the transmitted OPO pulses (frequency, spectral profile) are controlled by means of the FRU, indicated as the green box in Figure 4a. To ensure narrow-band and spectrally stable operation of the OPO, its cavity must be matched to the frequency of the seed lasers. A CH_4-gas cell in combination with an interferometric standard serves as a frequency-calibrated wavemeter. This enables spectral control of both the seed lasers and transmitted pulses on a shot-by-shot basis. As outlined in Section 3, the IPDA Lidar method is not free from "internal" radiometric calibration needs and requires the

knowledge of the ratio of outgoing online and offline pulse energies at similar accuracy as requested for the measurement of the Lidar signals. In order to account for ageing of the detector, this measurement will be performed by the same Lidar detector. For this purpose, an integrating sphere is used to attenuate the calibrating laser beam to a power level that is comparable to the received Lidar signals. Initial breadboard studies revealed that this concept for the relative pulse energy measurement in principle works well, but at the expense of introducing a further error source. The integrating sphere gives rise to a speckle pattern, which is not stationary within the relevant timing sequence (~7 s) due to small temperature drifts. Investigations show that this kind of error source can sufficiently be suppressed through the implementation of a synthetic high frequency speckle generator. Such device can be regarded as an additional white noise source and therefore does not increase systematic errors in the IPDA Lidar measurement [89].

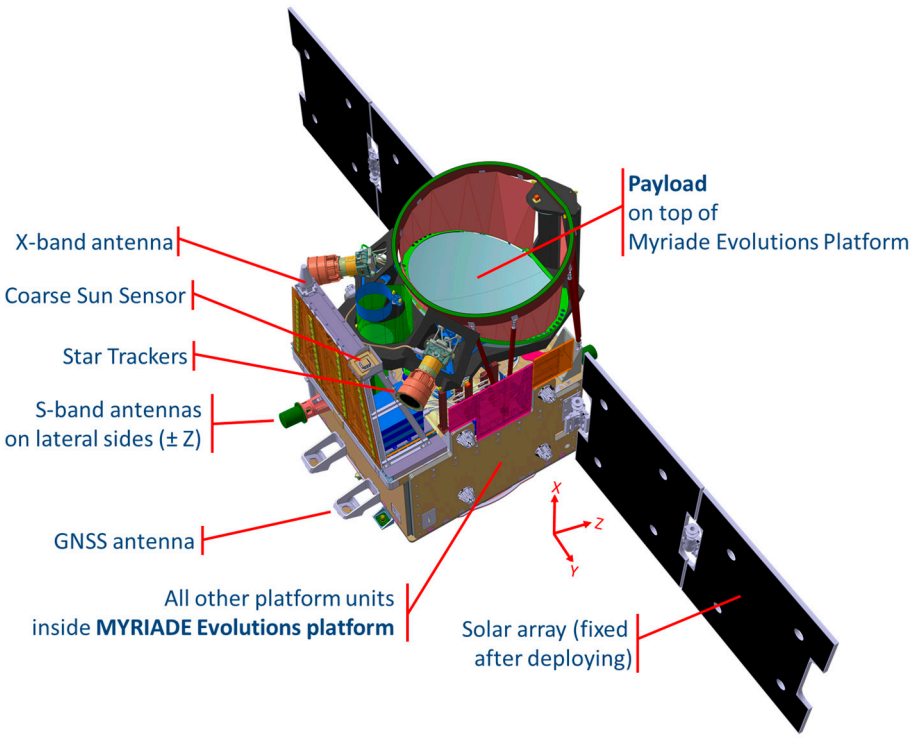

Figure 3. MERLIN satellite with the IPDA Lidar instrument from DLR attached on the MYRIADE evolution platform from CNES. Copyright Airbus Defence and Space.

Further optical elements, which will be traversed by the outgoing beam, include the Active Pointing Control (APC) and the transmitter telescope to ensure that the outgoing OPO pulses are centred on the telescope receiver footprint of about 200 m in diameter. For the latter, an off-axis Cassegrain-like telescope (with a diamater of about 69 cm) in bi-static configuration has been selected. This configuration satisfies both the scientific requirements of a large signal collection area and possible launch constraints for a piggyback satellite, which calls for a rather compact instrument in the x-direction (see Figures 3 and 4a). The collected signals pass an optical filter for background light rejection and are focused on a low-noise, single-pixel detector with a relative large sensitive area of about 200 µm (circular diameter). For MERLIN, a commercially available Avalanche Photo Diode (APD) that does not require extra cooling was chosen as the detector. To fulfil the demanding measurement performance, an intensive evaluation and critical selection program in connection to breadboard activities has been initiated and will continue over the development phases of the instrument. The goal is to select the best-qualified device on the market.

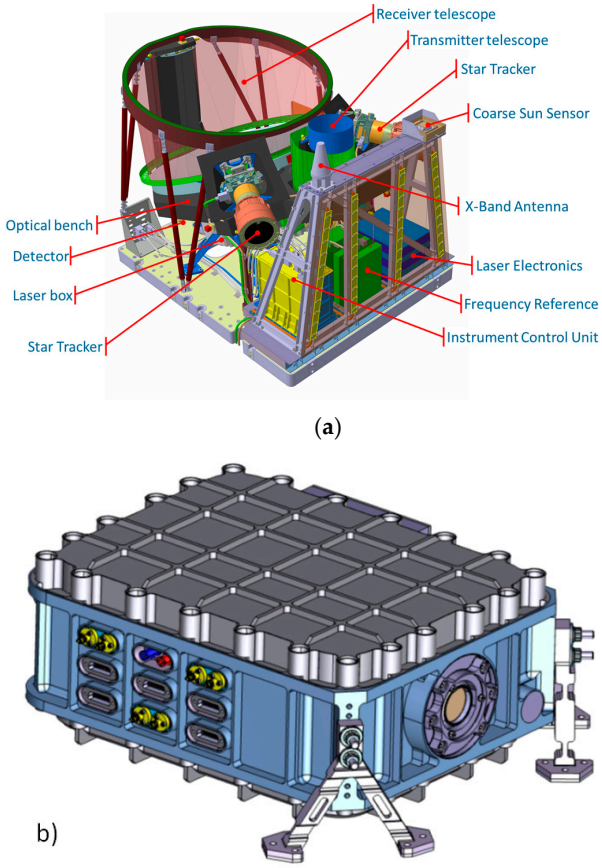

Figure 4. (**a**) IPDA-Lidar instrument with all subsystems integrated, (**b**) assembled laser head (will be mounted upside down on the optical bench). Copyright Airbus Defence and Space.

With respect to operations, the instrument will collect data without interruptions all over the orbit. The targeted pulse-pair sampling rate is 20 Hz, while the pulse energy for each OPO pulse amounts to 9.5 mJ. The overall sizing of these major instrument parameters was driven by the needs to fulfil the observational requirements and to fit platform resources and overall mission costs. The proposed transmitter concept is expected guarantee stable instrument operation throughout the envisaged mission lifetime of 3 years. With respect to timing, the round-trip time of the emitted pulses and received echoes from the Earth's surface is about 3.4 ms for a 500 km orbit height. Since only one detector unit is used, the online and offline pulses are not transmitted simultaneously. A temporal separation of about 250 µs will be applied to avoid possible signal ambiguities due to interfering Lidar signals from polar stratospheric clouds (PSC) or strong aerosol layers in the stratosphere after a big volcanic eruption. As a result of this small time delay, the online and offline ground spots will be separated by about 2 m, which is regarded as negligible compared to the spot diameter of about 100 m (90% of encircled energy). The maximum sampling distance between two shot-pairs of the MERLIN measurements amounts to about 350 m, which is given by the ground spot velocity of about 7 km/s and the pulse-pair sampling rate of 20 Hz. Single shot- pairs are then averaged during the on-ground processing on 50 km windows (about 142 shot- pairs).

The near infrared spectral region around 1.6 microns was preselected to minimize the sensitivity to atmospheric temperature and aerosol loading and cross-sensitivities to other trace gases (mainly CO_2 and H_2O). Four candidate line multiplets and associated pairs of online/offline frequencies were identified and considered. The final choice is the R6 multiplet at a frequency of 6077 cm^{-1} (corresponding to 1.645 µm in vacuum), which promises higher measurement sensitivity to CH_4 molecules residing in the planetary boundary layer (PBL). In reference to the A-SCOPE study,

the decision was based on calculation of a scaling factor for each candidate line that expresses the fractional amount of absorption taking place in the PBL (e.g., up to 850 hPa [86]. It turned out that the preferred R6 multiplet yields a scaling factor that is 25% to 35% larger with respect to the other candidate lines, and about 23% with respect to an instrument with a constant weighting function (as illustrated in Figure 5).

A further important aspect for implementation of the envisaged payload is the need to minimize systematic errors that may arise from "small" laser frequency instabilities or unknown Doppler shifts caused by instrument/satellite pointing errors. These mainly spectral-based error sources can seriously impact the systematic error budget of IPDA Lidar measurements, as analyzed to some depth in the framework of the A-SCOPE report for CO_2 [86]. In the case of MERLIN, however, a dramatic relaxation of the required frequency knowledge can be achieved by tuning the online position close to the trough minimum of the one-way optical depth spectrum, as illustrated in Figure 5. For this frequency position, the measured DAOD is rather immune to small changes of the laser frequency, as shown by the derivative function with respect to frequency. Further details of the error budget are given in Section 5.

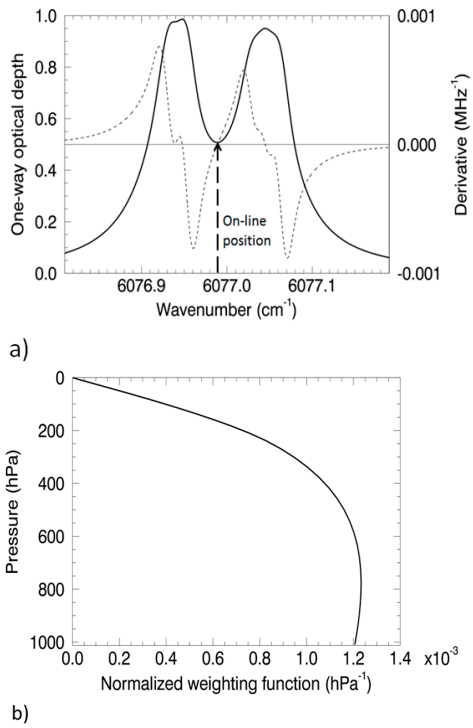

Figure 5. (**a**) One-way optical depth (thick black line) and its first derivative (thin dashed line) for the selected R6 multiplet around a frequency of 6077 cm^{-1}. The simulation is based on Voigt-profile calculations using the HITRAN database with US Standard Atmosphere. The thin solid line corresponds to the one-way optical depth for selected on-line frequency marked by the dashed arrow. (**b**) Corresponding pressure-based weighting function for the selected online frequency.

The platform considered for MERLIN strongly benefits from the MYRIADE Evolutions Program, which is an enhancement with respect to the original MYRIADE concept of small satellite series. The new concept offers the MERLIN instrument payload to allocate more power (around 150 W) and a greater mass (around 140 kg). The bus structure is a rectangular parallelepiped with dimensions of $98 \times 102 \times 58$ cm^3. The main improvements are a new structure compatible with a satellite mass up to 470 kg (limited to 430 kg on MERLIN due to launcher capacities); an increased solar array capacity and power supply; a more effective propulsion system; an improved Attitude and Orbital Control System (AOCS); an increased capacity for payload data storage; improved reliability figures, and; obsolescence handling and finally compatibility with low orbits (addressing atomic oxygen issues).

The Lidar payload is housed on the upper panel of the platform. Some platform units are located close to the instrument: two star tracker optical heads with their baffle, two solar arrays, one X-band antenna and a sun sensor notably to take into account a sun avoidance mechanism.

4.2. Mission Orbit

The selection of the MERLIN orbit (see Figure 6) is driven by the following considerations. To reduce sampling biases in the estimation of the methane sources, rather homogeneous measurement coverage in space and time is generally preferred. Of particular importance are measurements over ecosystems such as tropical and boreal wetlands, which are poorly monitored by the existing surface network. In practice, however, the measurement coverage of a Lidar will be limited by the overpass positions and frequency, and the presence of optically thick clouds. As an optimal compromise, a near-polar orbit to observe all latitude zones providing good samples of all climate zones over the continents and the oceans has been chosen. Even though the sampling of diurnal variations is not the focus of the mission, the choice of a sun-synchronous orbit at a local time of the ascending node LTAN = 06:00 or 18:00 appears preferable. At these times, the relatively stable sun-illumination condition and, therefore, stable thermal environment, helps to mitigate possible biases related to instrument frequency drifts or transmitter pointing issues. At both 06:00 and 18:00 local time, the low sun elevation angle reduces the amount of solar flux reflected from the surface to the satellite and thus limits the noise caused by the background light. Of key importance is the selection of a low orbit height of about 500 km in order to maximize the signal strengths that directly impacts measurement precision considering the limited power of the OPO. Orbit cycling of 28 days allows for overpasses within a circle of 50 km of all ground reference stations (notably TCCON) on a monthly basis which will help the long-term validation of the satellite measurements. The eclipse phase will be $\leq$20 min for each orbit during winter times, which in principle allows continuous operation of the instrument throughout the mission. All relevant orbit parameters are listed in Table 2.

Table 2. Satellite and orbit parameters for MERLIN. Optical Parametric Oscillator (OPO).

Platform	MYRIADE Evolutions
Satellite Mass (Platform+Payload):	430 kg
Satellite Power (Platform+Payload):	500 W
GPS receiver:	2 sensors
Star tracker:	2 optical Heads
Payload:	IPDA Lidar for Methane
Mass allocation:	140 kg
Power allocation:	150 W
Laser transmitter type:	Nd:YAG pumped OPO
Online frequency:	6076.9896 cm^{-1}
Offline frequency:	6075.97 cm^{-1}
Pulse energy:	9.5 mJ
Pulse length:	20 ns
Time lag between on/offline transmission:	250 µs
Pulse-pair repetition rate:	20 Hz
Receiving telescope size:	69 cm
Detector type:	Avalanche Pin Diode (APD)
Spot size on ground	100 m (90% encircled energy)
Orbit:	Sun synchr. polar, low Earth orbit (LEO)
LTAN:	06:00 h or 18:00 h
Height:	~500 km
Inclination:	97.4°
Repeat cycle:	28 days
Attitude control:	3 axis stabilized

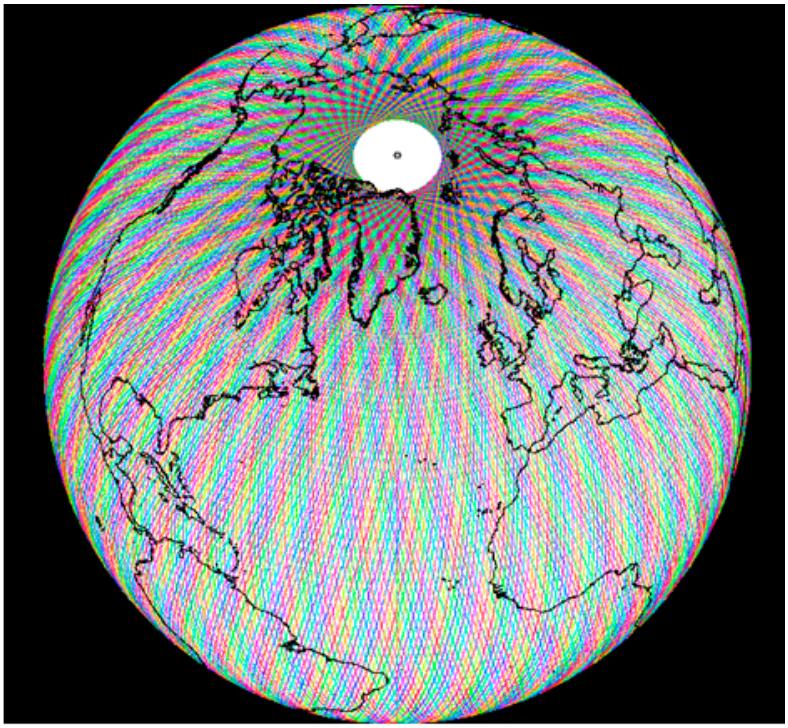

a)

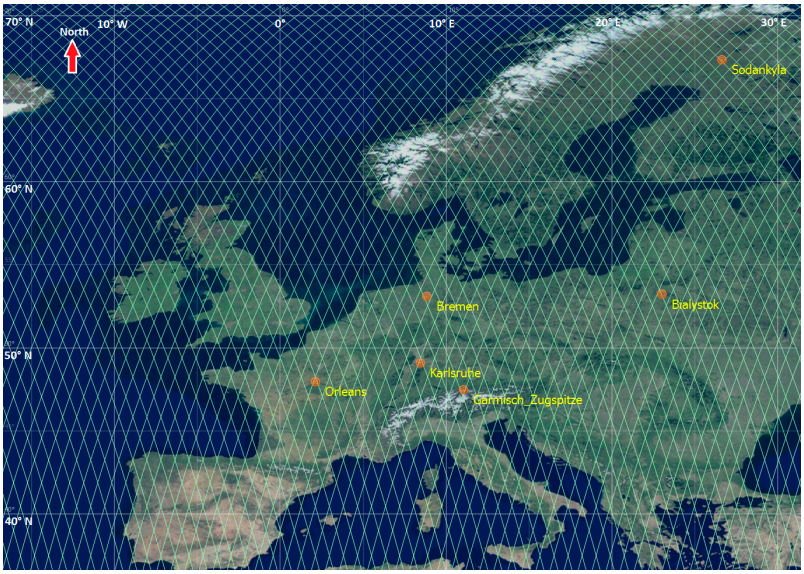

b)

Figure 6. (**a**) Example of global ground track density for the 28-day repeat cycle. (**b**) Ground track density over Europe per month. The yellow spots indicate the Total Carbon Column Observing Network (TCCON) ground reference stations considered for long-term validation.

4.3. Data and Products

The precise measurements performed by MERLIN require a careful processing, with reliable algorithms, to ensure the final performance of the mission. A Payload Data Processing Centre (PLDP) will operationally produce and distribute the official products of the mission to the users by request. The level 1 to level 3 products will be made publicly available, while access to the level 0 data will

be restricted to expert users. In the following the individual products and processing steps are briefly described.

Level 0 (L0) data consist of raw data containing the backscattered signals for each individual laser shot pair, auxiliary data, and some geometric information (latitude, longitude) in a chronological data sequence. The ordering of the data and its cutting into individual products of one orbit is done in this L0 processing step.

Level 1a (L1a) products consist of vertically resolved, pulse energy corrected Lidar data on a shot-by-shot basis. The processing steps include removal of background signals and performing minor non-linearity corrections. The vertical sampling of this product is 2 m below an altitude of about 3 km. This corresponds to the length of the range bin given by the speed of the Analog-Digital-Converter (ADC), which is 75 MHz. It is 50 m (sum of 25 range bins) between 3 and 20 km and 200 m (sum of 100 range bins) between 20 and 40 km, respectively. The vertical resolution of the Lidar signals (e.g., the length of uncorrelated vertical backscatter signals) is 30 m, which is given by the limited bandwidth of the detection electronic chain. L1a product will be complemented by the ensemble of parameters that are necessary to go from L0 data to L1a product. This complement will be gathered as the level 1p data and distributed to experts on request.

Level 1b (L1b) products consist of DAOD values both on single shot-pair basis and for an averaging window (nominal 50 km to improve the signal-to-noise ratio (SNR), about 142 shot- pairs). The first processing step is to retrieve the range distance from satellite to the hard target, which is done by a sophisticated search of the maximum value using the offline measurement due to the higher SNR. An integration of the vertical signal around the hard target echo provides the signals $P_{off,on}$ from Equation (1) and a similar algorithm yields $E_{off,on}$. The DAOD is then computed for each shot-pair. The retrieved range, combined with knowledge of the altitude and attitude of the spacecraft, also serves to refine the geolocation and determine the SSE. Once this shot-by-shot processing is performed, an average value of DAOD for a window of 50 km is computed, combining about 142 shot-pairs [66,90]. Note that the averaging distance might change in accordance to a changing albedo. A clear sky only averaging is also realized.

Level 2 (L2) products consist of the column-weighted dry-air mole fraction of methane (XCH_4), at the scale of both single shot-pairs and across the averaging window. The processing includes NWP analyses to obtain the pressure, temperature and humidity information needed to apply Equations (3) and (4) and compute the weighting function. The random error associated with XCH_4 is also computed. For the averaged product, the last processing step consists of removing the bias introduced by the averaging of noisy signals [91].

Level 3 (L3) products consist of XCH_4 maps. Processing incudes the visualisation of the L3 products using gap-filling and comparison with independent distant XCH_4 measurements. A Kalman-filtering algorithm, as described in [80], will be applied.

Aside from these data products directly delivered by the MERLIN mission, level 4 (L4) data products are methane surface fluxes at various temporal and spatial scales, obtained through assimilation in transport models. Level 4 data products will be provided by scientists at various scientific research institutions using lower level MERLIN data.

In the context of the overall mission objective, additional geophysical products can be derived from MERLIN mission using the above mentioned L1a products. They might provide information about the surface (topography, estimates of the vegetation height and occasionally information on the vertical structure, Lidar retro-reflectance) and the atmosphere (cloud boundaries, including cloud base for small-to-moderate cloud optical thickness). Their retrieval will be left to individual scientific groups worldwide.

4.4. Validation

The overall goal of validation is to assess the usefulness of the main MERLIN products for their intended scientific application [90]. In practice, the MERLIN data and products will be compared

to temporally and spatially coincident measurements performed by independent instrumentation from various platforms and from a variety of locations around the globe. To infer the data quality over the mission lifetime, both long-term and campaign-based validation activities are foreseen. For this, the full suite of the existing, high-accuracy and reliable techniques, including flask sampling and remote sensing, will be used (e.g., [3,12,24]). The Total Carbon Column Observation Network (TCCON), which has been developed and already successfully deployed for validation of space-based passive GHG sensors, is regarded as a beneficial validation infrastructure, since it consists of various stations distributed over the globe [12]. Of particular importance for validation are balloon-borne and airborne in situ sensors, both providing profile information on CH_4, which can be converted to XCH_4 using Equation (3) (e.g., [8,11]). In situ sensors provide the most accurate data calibrated against the WMO standard, thus promising the highest level of confidence [24]. Furthermore, aircraft are quite flexible, providing temporally and spatially coincident measurements almost anywhere on the globe (e.g., in data-sparse regions without any information, or far away from ground-based measurements). The validation of the DAOD (L1b) products will benefit from co-located flights with the airborne MERLIN demonstrator CHARM-F introduced in Section 1 [66]. This instrument will use identical measurement frequencies and a similar viewing geometry for a direct inter-comparison of the airborne DAOD values to the MERLIN observations, which is particularly helpful for validation over orographically structured terrain and areas with changing surface reflectivity. In the case of the high-flying HALO aircraft (up to 15 km altitude), about 95% of the CH_4 column as seen by MERLIN can be captured by airborne validation. The remaining part of the profile (above the aircraft) will be taken from simulations of state-of-the-art atmospheric chemistry and transport models, as well as from co-located in situ profiles acquired by balloons. In order to fly more frequently, the installation of CHARM-F on the SAFIRE (Service des Avions Français Insrumentés pour la Recherche en Environnement) Falcon aircraft will be considered. Synergies of validation with other space missions scheduled for the early 2020s are also foreseen (e.g., GOSAT II, Sentinel 5P, MICROCARB for CO_2 and IASI-NG for broader atmospheric composition).

5. Performance

The main, albeit indirect, scientific objective of the MERLIN mission is to reduce uncertainties on CH_4 sources and sinks, from global to regional scales. This is done through atmospheric flux inversions, using the information (L2 products) on atmospheric CH_4 columns (XCH_4) provided by MERLIN (see introduction and Section 2). To be confident in these uncertainty estimations, a multi-model assessment is necessary accounting for the full error budget for L2 XCH_4, including both random and systematic errors.

5.1. XCH_4 Error Budget

The random error is usually defined as the part of the error which tends towards zero when enough independent data are accumulated. For practical issues, in order to get a definition that can be easily handled when estimating the instrument error budget, we define the random XCH_4 error as the part of the error with spatial and/or temporal evolution at high frequency (i.e., >1 Hz), with zero mean over the mission lifetime, and the systematic error as either varying at low frequency (i.e., <1 Hz), or being dependent on the scene observed. This ensures that the random error is strictly non-correlated between two measurements (defined after a 50 km averaging, thus separated by about 7 s). Consequently, the horizontal averaging of data described in Section 4 leads to a reduction of error by square root of N, with N being the number of shot-pairs considered in the averaging process. Table 3 shows the user requirement related to these two types of errors.

Table 3. User requirements for MERLIN (1-sigma error). * The values in brackets correspond to the actual targets after applying a correction factor of 1.23 to account for the actual MERLIN weighting function with enhanced sensitivity in the boundary layer (see text).

Parameter	User Requirements			MERLIN System Specification Requirement
	Threshold	Breakthrough	Target	
XCH_4 random error	36 ppb	18 ppb	8 ppb	22 ppb (27 ppb *)
XCH_4 systematic error	3 ppb	2 ppb	1 ppb	3 ppb (3.7 ppb *)
Spatial coverage	Global	Global	Global	Global
Resolution	Horizontal: 50 km averaging; vertical: total column			

The "threshold" requirement is the minimum requirement to ensure that the MERLIN products are useful for CH_4 emission retrievals by inverse modeling. The "breakthrough" requirement is an intermediate requirement level that provides a significant improvement to the current satellite observation system and, given the current status of the instrument development, is regarded as the optimum from a cost-benefit point of view. The "target" requirements represent a tremendous improvement relative to what is achieved today and may be achieved by a follow-on MERLIN-type instrument. We note that the requirements in Table 3 apply to a total column with vertically constant weighting function. As illustrated in Figure 5b, MERLIN's online frequency has been chosen to obtain a weighting function with enhanced sensitivity in the boundary layer (about at least 1.23 higher than in the upper part of the atmosphere), yielding more variability in the XCH_4 retrieval. This offers the possibility to relax the requirements applying to MERLIN in Table 3 by a factor 1.23, making the actual targeted random error to be better than 27 ppb and the actual targeted systematic error better than 3.7 ppb (A-SCOPE-Report for CO_2, Figure 4.1, p. 43 in [86]). The actual target for random errors is between threshold and breakthrough values of the user requirements (Table 3). The (already ambitious) actual target for systematic errors is at the threshold level.

The MERLIN system specification requirements (column 5 of Table 3) result from parameter analysis of the various error contributors as described in the following. As the processing of MERLIN data up to level 2 can be written in a fully analytical form, the error budget is estimated mostly through an analytical approach based on derivative computations from Equations (1)–(4). The random error on XCH_4 mostly depends on the random error of the measured DAOD, coming from the signal-to-noise ratio of the instrument. The error contributors to XCH_4 from the weighting function, such as the random part of the error from Numerical Weather Prediction (NWP) external data (temperature, surface pressure and humidity) or from spectroscopy, or from the target Scattering Surface Elevation (SSE) estimation, are negligible. Indeed, an upper estimate of the random error part arising from surface pressure (from NWP models and SSE) and spectroscopy errors is about 5 ppb compared to about 20 ppb for instrument-related errors. As the errors must be summed up quadratically, this contribution can thus be neglected. The error from the DAOD itself comes from several contributors, the first being the instrument noise. Half of it comes from detector noise, and the other part from amplifier noise and signal shot noise. Thanks to the orbit selection (dawn-dusk), the solar contamination is rather low and the background signal shot noise is almost always negligible. Other potential error sources such as speckle noise and the noise from internal calibration chain have been minimized by design of these subsystems, as outlined in Section 4.

The main part of the random error depends on the geophysical situation: It is mainly related to the surface reflectivity and to the aerosol load, which directly relates to the signal strength, and secondly to the surface pressure and other elements with minor impact (e.g., slope of terrain, CH_4 concentration, solar elevation angle, etc.). The performances are given in Table 4 for a typical reference scene with reflectivity 0.1 sr^{-1} (typical of a vegetation surface), a median aerosol load, and a SSE (related to surface pressure) of 300 m, which corresponds to median altitude over land. A worst-case situation corresponds to sea and snow areas, where the 50 km random error might reach 50 to 100 ppb. In that case, the random error can be reduced by further averaging.

Table 4. Total budget for XCH_4 random error obtained by combining specified values for contributors. The current best estimate of the budget (24.3 ppb) is compliant when accounting for the actual weighting function with enhanced sensitivity in the boundary layer (27 ppb, see Table 3).

Parameter	Random Error	Impact on XCH4
Differential Atmospheric Optical Depth (DAOD)	1.3%	23.14 ppb
SSE	10 m	2.57 ppb
Surface pressure (Numerical Weather Prediction (NWP))	2 hPa	4.27 ppb
Temperature	2 K	5.2 ppb
Total budget based on specified values		24.3 ppb

For the systematic error, the situation is rather different than for the random error. Indeed, as shown in Table 5, there are many contributors, which have roughly the same magnitude: (i) the DAOD measured by the payload; (ii) the error on the surface pressure; and (iii) the error on the weighting function. The first one is caused by the yet limited variations of the on/off ratio between the atmospheric and the internal calibration path, and by the as-yet-unknown residual of non-linearity after the correction of the detector. The second one comes from both the uncertainty of NWP products and the error of SSE estimation (including platform altitude, attitude and Lidar ranging contributors). Regarding the third contributor, the cross-section knowledge depends on external parameters (temperature profile from NWP, spectroscopic parameters), but also of the Lidar itself, through the knowledge of the emitted frequency. As explained in Section 3, the "online" frequency has been chosen to be in a local minimum of the CH_4 manifold in order to reduce the sensitivity to laser stability. Moreover, the Doppler effect is minimized by the choice of an across-track pointing angle of $-1°$, for which the Doppler effects caused by the Earth rotation and the satellite movements almost compensate (a negative sign means the line-of-sight points east at the Ascending Node). Thus, the residual frequency error resulting from our limited knowledge of FRU measured frequency and the Doppler effect is almost negligible. For the error arising from the use of humidity profiles obtained from NWP, an optimal position of the offline wavelength guarantees a minor impact, due to compensating effects between the error impact on the water vapor DAOD corrective term and on the weighting function, as explained in chapter 3. Finally, the processing itself may contribute to the systematic error through the introduction of scene-dependent biases, for example in the horizontal averaging step [91].

Table 5. Total budget for XCH4 systematic error obtained by combining specified values for contributors. The current best estimate of the budget (3.1 ppb) is compliant to the observational requirements when accounting for the actual weighting function with enhanced sensitivity in the boundary layer (3.7 ppb, see Table 3).

Parameter	Systematic Errors	Impact on XCH4
DAOD	0.13%	2.31 ppb
SSE	6 m	1.54 ppb
Surface pressure (NWP)	0.2 hPa	0.43 ppb
Temperature	2 profiles of bias	0.5 ppb
Water vapor	4%	0.1 ppb
Methane cross section	0.2%	0.62 ppb
Frequency	7 MHz offset, 8 MHz systematic	0.3 ppb
Laser width knowledge	5% for 100 MHz	0.17 ppb
Spectral purity	-	0.23 ppb
Processing		1 ppb
Total budget based on specified values		3.1 ppb

The errors for individual contributors of Table 5 are obtained either from the basic equations of processing, or with more detailed simulations, for example for the errors related to frequency which

combine the uncertainty of the emitted wavelength, the FRU characteristics, the Doppler effect, and so forth. Then, they are summed quadratically as they are independent. A more detailed description of the modelling of the error is outside the scope of this paper and will be given in a further publication.

5.2. Random and Systematic Error Scenarios

In order to transfer the errors on level 2 products to errors on flux estimates (level 4), global spatial and temporal patterns of both random and systematic errors have been generated for cloud-free observations.

As explained above, the random error mainly depends on the signal intensity measured by the instrument that depends on the ground reflectance and atmospheric transmission. Thus, the random error maps of level 2 data are obtained as a simple function of surface reflectance and aerosol optical depth, both provided by observations with the Moderate Resolution Imaging Spectrometer (MODIS) which is operated on NASA satellites.

Through the analysis of the root cause of systematic error, geographical patterns have been attributed to each component of the systematic error (e.g., the error on SSE coming from limited knowledge of the platform exact altitude is expected to lead to orbital effects and thus produce a systematic error pattern linked to latitude). The six following individual patterns were defined: seasonal; latitudinal; proportional to surface pressure; proportional to topography variations, and; proportional to the product of surface albedo and atmospheric transmission. The amplitude of each pattern of systematic error was obtained by analysis of the error budget. By combining the six individual patterns with + or − signs, we obtained a full set of 32 different mixed scenarios of systematic error global maps. A detailed description of the error patterns on global basis will be given in a dedicated study of a follow-on paper.

5.3. Expected Uncertainty Reductions on Surface Emission

The spatially distributed scenarios of random and systematic errors described above for MERLIN have been integrated into an atmospheric inversion simulator that converts uncertainties in XCH_4 into uncertainties on surface emissions using an inversion system (based on [92]). This simulator has the originality to carry both random and systematic error (Philippe PEYLIN, pers. Comm.). Although relatively marginal at sounding level (±3.7 ppb on global scale, value from the MERLIN system specification requirement), the systematic errors have a larger influence than the random errors on the regional CH_4 emission estimates because they are not reduced by data averaging accounting for both types of errors. Expected uncertainty reductions on CH_4 emissions are found on average to be 59% for the continental tropics (30°S–30°N), 84% for continental mid-latitudes (30°N–50°N), and 53% for continental high latitudes (above 50°N, Figure 7). The largest uncertainty reductions are achieved for temperate regions. Uncertainty reductions obtained for the aggregated boreal regions is 53% on average, indicating that MERLIN still brings constraints for high northern latitudes, contrary to most passive SWIR missions. For tropical regions, the score for uncertainty reduction is mostly influenced by desert regions and the choice to distribute systematic errors partly on albedo to represent potential driver of nonlinearity effect of the MERLIN detector. More details and regional analyses will be provided in follow-up papers.

Unsurprisingly, once the instrument is flying, systematic errors are expected to be the main limiting factor to use XCH_4 to reduce uncertainties on CH_4 emissions. Nevertheless, the MERLIN error budget presented here is considered an important step towards anticipating the major causes and magnitudes of MERLIN systematic errors. Using validation measurements, it should be possible to correct some of these systematic errors, thus reducing their impact on the error budget. Most surely, some other unexpected errors will appear or expected ones will be different in their space-time distribution or magnitude. Although the ambitious systematic error targeted by MERLIN calls for caution before the mission is operating, these first results on the end-to-end error budget of MERLIN

are very encouraging, highlighting the ability of MERLIN to provide useful information for the global CH_4 cycle.

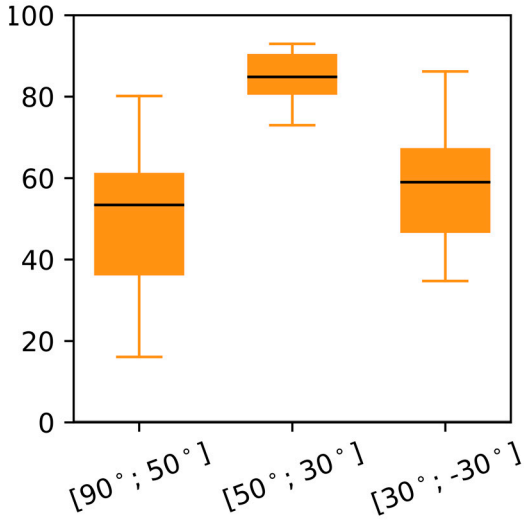

Figure 7. Uncertainty reduction on methane emission (%, y-axis) for three latitudinal bands (x-axis) for MERLIN (orange) using the scenarios developed to represent MERLIN random and systematic errors. Sahara pixels, with very low methane flux and high albedo, have been removed from the 30°N-30°S barplot.

6. Conclusions

The overall goal of the French-German Climate Mission MERLIN is to reduce uncertainties on our knowledge of the global methane budget. For this purpose, the scientific objective is to deliver observations of atmospheric methane from space for all latitudes using a satellite based on an innovative Lidar instrument. The programmatic goal is to develop, launch and operate this satellite in French-German cooperation to provide relevant information about the global CH_4 cycle. Since atmospheric CH_4 is the second-most important anthropogenic greenhouse gas, MERLIN will give insight into the nature and variety of its sources which will offer interesting opportunities in the context of climate change—also the context of the implementation of the Paris Agreement signed during COP21 in December 2015.

MERLIN will deliver column-weighted dry-air mole fractions of CH_4, referred to as XCH_4, along the satellite sub-track (level 2 product) with arandom error better than 27 ppb (50 km averaging along the satellite track) and a (1-sigma) systematic error of better than 3.7 ppb. The mission serves as a scientific and technological demonstrator for a trace gas Lidar in space that will use the differential absorption measurement principle. The low-biased data will be highly useful to the scientific community, especially for atmospheric inversions estimating CH_4 emissions from XCH_4 products. In particular, the mission will provide complementary information to the ground-based network and to passive satellite sensors that are limited either by insufficient sunlight (NIR-sensors) or lack of sensitivity to CH_4 molecules in the planetary boundary layer (PBL) (IR-sensors). The combined use of different data sets (including in situ observations) in a single model parameter optimization framework offers the perspective of applying the concept of carbon cycle data assimilation (e.g., [93]) to CH_4. Such a combined use of different data sets in a consistent manner will certainly be challenging, but potential inconsistencies will provide directions for improvements.

The methodology proposed for the MERLIN observations is well demonstrated by ground-based and airborne measurements. It involves the measurement of the DAOD using Lidar signals at two distinct frequencies in the vicinity of a CH_4 absorption line originating either from ground or cloud top as the target. The measured DAOD values are converted to XCH_4 by means of auxiliary

meteorological data from NWP and spectroscopic information. To observe all latitude zones for year-round observations, a sun-synchronous, near-polar orbit was selected.

The MERLIN space segment is comprised of a mini-class satellite carrying only one scientific instrument, which is the IPDA Lidar system operating in near-nadir-viewing configuration. A Nd:YAG pumped OPO will serve as the MERLIN transmitter operating in the 1.64 μm spectral domain. The platform benefits from the French MYRIADE Evolutions Program, which is an enhancement of the original MYRIADE concept of small satellite series. The development of the payload also benefits from CHARM-F, the airborne MERLIN demonstrator and from European space laser development efforts at ESA and DLR (ALADIN, ATLID, FULAS).

MERLIN provides three levels of products, which will be made publicly available. Level 1 processing comprises vertically resolved Lidar data up to a height of 40 km at three different vertical sampling rates, as well as the generation of DAOD products on different horizontal averaging intervals (baseline is 50 km). Level 2 processing yields XCH_4 and level 3 products will consist of corresponding maps using an original Kalman-filtering algorithm.

The full suite of the existing, high accuracy and reliable techniques, including flask sampling and passive remote sensing (e.g., TCCON), will be used for validation of the MERLIN products as long as the mission is operating. Of particular importance for campaign-based validation are balloon-borne and airborne in situ sensors, as well as airborne remote sensors such as CHARM-F, the DLR's IPDA Lidar instrument operated onboard the German research aircraft HALO. The latter serves as an airborne demonstrator for MERLIN, as it uses identical transmitter frequencies and viewing geometry. To prepare for the validation exercise, a pre-launch campaign will take place, possibly involving both German (HALO) and French (SAFIRE) aircraft.

A first analysis of an end-to-end error budget revealed that the following CH_4 surface uncertainty reduction can be achieved by the MERLIN observations for the different regions: 59% for the continental tropics (without the Sahara dessert); 84% for continental mid-latitudes, and; 53% for continental high latitudes. This performance relies to nominal random errors, modelled with a dependency on the surface reflectivity and aerosol load (as a reference case, of 24.3 ppb on XCH_4, dominated by the DAOD related error with an impact of 23.1% on XCH_4). The situation is quite different for the calculated systematic error budget of 3.1 ppb where several contributors show similar errors. However, the largest impact of 2.3 ppb arises from assumed detector non-linearity. Uncertainty reductions obtained here for the aggregated boreal regions (+53% on average) indicates that MERLIN observations will further constrain flux estimates at high northern latitudes, contrary to most passive missions.

A successful MERLIN mission will provide the first low-bias, global, spaceborne IPDA Lidar data for an anthropogenic greenhouse gas, allowing for the significant improvement of our knowledge of the global CH_4 budget. The MERLIN mission will open the path for future active remote sensing missions dedicated to the monitoring of greenhouse gases from space.

Acknowledgments: We are grateful to CNES and DLR who selected MERLIN in 2010 as a future climate mission based on a dedicated Lidar instrument for the measurement of atmospheric methane for the first time. Special thanks are given to the members of MERLIN project teams from French CNES (Carole Deniel, Frédéric Estève, Eric Julien, Jordi Chinaud, Caroline Bès, Francesc Tintó, Pascale Moro, Clémence Le Fèvre, Etienne Montagnon, David Ducros), from French LMD (Raymond Armante, Vincent Cassé, Olivier Chomette, Dimitri Edouart, Ha Tran, Thibault Delahaye, Jean-Michel Hartmann, Yoann Tellier, Sébastien Berthier), from French groupe de spectrométrie moléculaire et atmosphérique (GSMA) (Virginie Zeninari, Raphael Vallon, Bertrand Parvitte), from French small and medium-sized enterprises (SMEs): NOVELTIS (Cédric Bacour), CAPGEMINI (Fabien Marnas), MAGELLIUM (Emmanuel Hillairet, Frédéric Nahan), SYNERGIE (Antonin Deville), from DLR Raumfahrtmanagement (Achim Friker, Dominik Maxein, Inés Usandizaga, and Hermann Berg, Christian Stephan), DLR Institut für Physik der Atmosphäre (Axel Amediek, Mathieu Quatrevalet, Christoph Kiemle), DLR Institut für Methodik der Fernerkundung (Thomas Trautmann, Günter Lichtenberg, Mourad Hamidouche), Deutsches Fernerkundungsdatenzentrum of DLR (Erhard Diedrich, Stephan Kiemle, Kai Wendlandt), and Airbus Defence and Space in France and Germany with their suppliers, who all strongly support the mission development during the subsequent phases. Error budget calculations have been possible thanks to CNES, CEA (LSCE) and national (GENCI TGCC) computational means. MERLIN is supported by the Federal Ministry of Economy and Energy on

the basis of a decision by the German Bundestag and the French Ministère de l'Enseignement supérieur, de la Recherche et de l'Innovation.

Author Contributions: The authors are all members of the MERLIN Science Advisory Group and therefore responsible for the content of the manuscript. Their particular contribution to the manuscript is given as follows: Gerhard Ehret*: Drafting Sections 1, 3, 4 and 6, Figures 1, 2 and 5, input references, drafting acknowledgement. Philippe Bousquet: Drafting Sections 1, 2, 5 and 6, input Figure 7, Table 1, abstract, writing list of references; Clémence Pierangelo: Drafting Sections 4 and 5, drafting Tables 3–5, input to list of references. Matthias Alpers and Bruno Millet: Input Figures 3 and 4, Table 2, input corrections of numbers in Section 4, acknowledgement. Jim B. Abshire, Andreas Fix, Pierre Flamant, Fabien Gibert, Patrick Rairoux: data input, update of writing of the methodology and technical paragraphs in Sections 1, 3 and 4, input to list of references. Frédéric Chevallier, Julia Marshall and Philippe Ciais, and Patrick Jöckel: Update of the full manuscript in the early phase. Input to Table 3 (MERLIN requirements definition) and data input Section 5, update list of references. Heinrich Bovensmann, John P. Burrows, Cyril Crevoisier, Anna Agusti-Panareda, Sander Houweling, and Marko Scholze. Update of the full manuscript of second draft. In particular Sections 1, 2, 5 and 6, update of list of references, polishing of the whole manuscript, input to Table 3 (MERLIN requirements definition). Christian Frankenberg, Birgit Heim, Martin Heimann, Hans-W Hubberten, Kathy Law, Alexander Löw and Torsten Sachs: Definition of the MERLIN observational requirements, data input to Table 3, data input to impact study Figure 7, input the list of references, polishing. Sebastien Payan and Martin Wirth: date input to Tables 4 and 5.

Conflicts of Interest: The authors declare no conflicts of interest.

References

1. Hartmann, D.L.; Klein Tank, A.M.G.; Rusticucci, M.; Alexander, L.V.; Brönnimann, S.; Charabi, Y.; Dentener, F.J.; Dlugokencky, E.J.; Easterling, D.R.; Kaplan, A.; et al. Observations: Atmosphere and surface. In *Climate Change 2013: The Physical Science Basis. Contribution of Working Group I to the Fifth Assessment Report of the Intergovernmental Panel on Climate Change*; Cambridge University Press: Cambridge, UK; New York, NY, USA, 2013.
2. Saunois, M.; Bousquet, P.; Poulter, B.; Peregon, A.; Ciais, P.; Canadell, J.G.; Dlugokencky, E.J.; Etiope, G.; Bastviken, D.; Houweling, S.; et al. The global methane budget 2000–2012. *Earth Syst. Sci. Data* **2016**, *8*, 697–751. [CrossRef]
3. WMO. World Meteorological Organisation, World Data Centre for Greenhouse Gases (WDCGG), Japan Meteorological Agency. Available online: http://ds.data.jma.go.jp/gmd/wdcgg/introduction.html (accessed on 31 March 2017).
4. Blake, D.R.; Mayer, E.W.; Tyler, S.C.; Makide, Y.; Montague, D.C.; Rowland, F.S. Global increase in atmospheric methane concentrations between 1978 and 1980. *Geophys. Res. Lett.* **1982**, *9*, 477–480. [CrossRef]
5. Sweeney, C.; Karion, A.; Wolter, S.; Newberger, T.; Guenther, D.; Higgs, J.A.; Andrews, A.E.; Lang, P.M.; Neff, D.; Dlugokencky, E.; et al. Seasonal climatology of CO_2 across north america from aircraft measurements in the noaa/esrl global greenhouse gas reference network. *J. Geophys. Res. Atmos.* **2015**, *120*, 5155–5190. [CrossRef]
6. Brenninkmeijer, C.A.M.; Crutzen, P.; Boumard, F.; Dauer, T.; Dix, B.; Ebinghaus, R.; Filippi, D.; Fischer, H.; Franke, H.; Frieβ, U.; et al. Civil aircraft for the regular investigation of the atmosphere based on an instrumented container: The new caribic system. *Atmos. Chem. Phys.* **2007**, *7*, 4953–4976. [CrossRef]
7. Schuck, T.J.; Ishijima, K.; Patra, P.K.; Baker, A.K.; Machida, T.; Matsueda, H.; Sawa, Y.; Umezawa, T.; Brenninkmeijer, C.A.M.; Lelieveld, J. Distribution of methane in the tropical upper troposphere measured by caribic and contrail aircraft. *J. Geophys. Res. Atmos.* **2012**, *117*, D19304. [CrossRef]
8. Chang, R.Y.W.; Miller, C.E.; Dinardo, S.J.; Karion, A.; Sweeney, C.; Daube, B.C.; Henderson, J.M.; Mountain, M.E.; Eluszkiewicz, J.; Miller, J.B.; et al. Methane emissions from alaska in 2012 from carve airborne observations. *Proc. Natl. Acad. Sci. USA* **2014**, *111*, 16694–16699. [CrossRef] [PubMed]
9. Paris, J.D.; Stohl, A.; Ciais, P.; Nédélec, P.; Belan, B.D.; Arshinov, M.Y.; Ramonet, M. Source-receptor relationships for airborne measurements of CO_2, CO and O_3 above siberia: A cluster-based approach. *Atmos. Chem. Phys.* **2010**, *10*, 1671–1687. [CrossRef]
10. Wofsy, S.; The HIPPO Science Team; Cooperating Modellers and Satellite Teams. Hiaper pole-to-pole observations (hippo): Fine grained, global scale measurements of climatically important atmospheric gases and aerosols. *Phil. Trans. R. Soc. A* **2011**, *369*, 2073–2086. [CrossRef] [PubMed]
11. Karion, A.; Sweeney, C.; Tans, P.; Newberger, T. Aircore: An innovative atmospheric sampling system. *J. Atmos. Ocean. Technol.* **2010**, *27*, 1839–1853. [CrossRef]

12. Wunch, D.; Toon, G.C.; Blavier, J.-F.L.; Washenfelder, R.A.; Notholt, J.; Connor, B.J.; Griffith, D.W.T.; Sherlock, V.; Wennberg, P.O. The total carbon column observing network. *Phil. Trans. R. Soc. A* **2011**, *369*. [CrossRef] [PubMed]
13. Gerilowski, K.; Tretner, A.; Krings, T.; Buchwitz, M.; Bertagnolio, P.P.; Belemezov, F.; Erzinger, J.; Burrows, J.P.; Bovensmann, H. Mamap—A new spectrometer system for column-averaged methane and carbon dioxide observations from aircraft: Instrument description and performance analysis. *Atmos. Meas. Tech.* **2011**, *4*, 215–243. [CrossRef]
14. Krings, T.; Gerilowski, K.; Buchwitz, M.; Hartmann, J.; Sachs, T.; Erzinger, J.; Burrows, J.P.; Bovensmann, H. Quantification of methane emission rates from coal mine ventilation shafts using airborne remote sensing data. *Atmos. Meas. Tech.* **2013**, *6*, 151–166. [CrossRef]
15. Krautwurst, S.; Gerilowski, K.; Jonsson, H.H.; Thompson, D.R.; Kolyer, R.W.; Thorpe, A.K.; Horstjann, M.; Eastwood, M.; Leifer, I.; Vigil, S.; et al. Methane emissions from a californian landfill, determined from airborne remote sensing and in-situ measurements. *Atmos. Meas. Tech.* **2017**, *10*, 3429–3452. [CrossRef]
16. Bousquet, P.; Ciais, P.; Miller, J.B.; Dlugokencky, E.J.; Hauglustaine, D.A.; Prigent, C.; Van der Werf, G.R.; Peylin, P.; Brunke, E.G.; Carouge, C.; et al. Contribution of anthropogenic and natural sources to atmospheric methane variability. *Nature* **2006**, *443*, 439–443. [CrossRef] [PubMed]
17. Houweling, S.; Kaminski, T.; Dentener, F.; Lelieveld, J.; Heimann, M. Inverse modeling of methane sources and sinks using the adjoint of a global transport model. *J. Geophys. Res. Atmos.* **1999**, *104*, 26137–26160. [CrossRef]
18. INFLUX. Indianapolis Flux Experiment. Available online: http://sites.psu.edu/influx/ (accessed on 25 August 2017).
19. Lamb, B.K.; Cambaliza, M.O.L.; Davis, K.J.; Edburg, S.L.; Ferrara, T.W.; Floerchinger, C.; Heimburger, A.M.F.; Herndon, S.; Lauvaux, T.; Lavoie, T.; et al. Direct and indirect measurements and modeling of methane emissions in Indianapolis, Indiana. *Environ. Sci. Technol.* **2016**, *50*, 8910–8917. [CrossRef] [PubMed]
20. Viatte, C.; Lauvaux, T.; Hedelius, J.K.; Parker, H.; Chen, J.; Jones, T.; Franklin, J.E.; Deng, A.J.; Gaudet, B.; Verhulst, K.; et al. Methane emissions from dairies in the los angeles basin. *Atmos. Chem. Phys.* **2017**, *17*, 7509–7528. [CrossRef]
21. Wong, C.K.; Pongetti, T.J.; Oda, T.; Rao, P.; Gurney, K.R.; Newman, S.; Duren, R.M.; Miller, C.E.; Yung, Y.L.; Sander, S.P. Monthly trends of methane emissions in los angeles from 2011 to 2015 inferred by clars-fts observations. *Atmos. Chem. Phys.* **2016**, *16*, 13121–13130. [CrossRef]
22. Locatelli, R.; Bousquet, P.; Saunois, M.; Chevallier, F.; Cressot, C. Sensitivity of the recent methane budget to lmdz sub-grid-scale physical parameterizations. *Atmos. Chem. Phys.* **2015**, *15*, 9765–9780. [CrossRef]
23. Patra, P.K.; Houweling, S.; Krol, M.; Bousquet, P.; Belikov, D.; Bergmann, D.; Bian, H.; Cameron-Smith, P.; Chipperfield, M.P.; Corbin, K.; et al. Transcom model simulations of ch4 and related species: Linking transport, surface flux and chemical loss with ch4 variability in the troposphere and lower stratosphere. *Atmos. Chem. Phys.* **2011**, *11*, 12813–12837. [CrossRef]
24. Dlugokencky, E.J.; Bruhwiler, L.; White, J.W.C.; Emmons, L.K.; Novelli, P.C.; Montzka, S.A.; Masarie, K.A.; Lang, P.M.; Crotwell, A.M.; Miller, J.B.; et al. Observational constraints on recent increases in the atmospheric ch burden. *Geophys. Res. Lett.* **2009**, *36*, L18803. [CrossRef]
25. Miller, S.M.; Wofsy, S.C.; Michalak, A.M.; Kort, E.A.; Andrews, A.E.; Biraud, S.C.; Dlugokencky, E.J.; Eluszkiewicz, J.; Fischer, M.L.; Janssens-Maenhout, G.; et al. Anthropogenic emissions of methane in the united states. *Proc. Natl. Acad. Sci. USA* **2013**, *110*, 20018–20022. [CrossRef] [PubMed]
26. Delahaye, T.; Reed, Z.; Maxwell, S.; Hodges, J.T.; Sung, K.; Brown, L.; Benner, C.; Devi, V.M.; Warneke, T.; Spietz, P.; et al. Precise methane absorption measurements in the 1.64 μm spectral region for the merlin mission. *J. Geophys. Res. Atmos.* **2016**, *121*, 7360–7370. [CrossRef] [PubMed]
27. Bousquet, P.; Ehret, G.; Group, M.S.A. *The MERLIN Science Plan*; CNES: Toulouse, France, 2015; Available online: https://files.lsce.ipsl.fr/public.php?service=files&t=9f79de7f3eabfe3655393efebef43377 (accessed on 25 August 2017).
28. GAW Report #213. In Proceedings of the 17th WMO/IAEA Meeting on Carbon Dioxide, Other Greenhouse Gases and Related Tracers Measurement Techniques (GGMT-2013), Beijing, China, 10–13 June 2013; World Meteorological Organization: Geneva, Switzerland, 2014.
29. Bovensmann, H.; Burrows, J.P.; Buchwitz, M.; Frerick, J.; Noël, S.; Rozanov, V.V.; Chance, K.V.; Goede, A.P.H. Sciamachy: Mission objectives and measurement modes. *J. Atmos. Sci.* **1999**, *56*, 127–150. [CrossRef]

30. Buchwitz, M.; De Beek, R.; Noel, S.; Burrows, J.P.; Bovensmann, H.; Schneising, O.; Khlystova, I.; Bruns, M.; Bremer, H.; Bergamaschi, P.; et al. Atmospheric carbon gases retrieved from sciamachy by wfm-doas: Version 0.5 co and ch4 and impact of calibration improvements on CO_2 retrieval. *Atmos. Chem. Phys.* **2006**, *6*, 2727–2751. [CrossRef]
31. Buchwitz, M.; Reuter, M.; Schneising, O.; Boesch, H.; Guerlet, S.; Dils, B.; Aben, I.; Armante, R.; Bergamaschi, P.; Blumenstock, T.; et al. The greenhouse gas climate change initiative (ghg-cci): Comparison and quality assessment of near-surface-sensitive satellite-derived CO_2 and CH_4 global data sets. *Remote Sens. Environ.* **2015**, *162*, 344–362. [CrossRef]
32. Burrows, J.P.; Hölzle, E.; Goede, A.P.H.; Visser, H.; Fricke, W. Sciamachy—Scanning imaging absorption spectrometer for atmospheric chartography. *Acta Astronaut.* **1995**, *35*, 445–451. [CrossRef]
33. Dils, B.; De Mazière, M.; Müller, J.F.; Blumenstock, T.; Buchwitz, M.; De Beek, R.; Demoulin, P.; Duchatelet, P.; Fast, H.; Frankenberg, C.; et al. Comparisons between sciamachy and ground-based ftir data for total columns of CO, CH_4, CO_2 and N_2O. *Atmos. Chem. Phys.* **2006**, *6*, 1953–1976. [CrossRef]
34. Frankenberg, C.; Aben, I.; Bergamaschi, P.; Dlugokencky, E.J.; Van Hees, R.; Houweling, S.; Van der Meer, P.; Snel, R.; Tol, P. Global column-averaged methane mixing ratios from 2003 to 2009 as derived from sciamachy: Trends and variability. *J. Geophys. Res. Atmos.* **2011**, *116*, D04302. [CrossRef]
35. Butz, A.; Guerlet, S.; Hasekamp, O.; Schepers, D.; Galli, A.; Aben, I.; Frankenberg, C.; Hartmann, J.M.; Tran, H.; Kuze, A.; et al. Toward accurate $CO(_2)$ and $CH(_4)$ observations from gosat. *Geophys. Res. Lett.* **2011**, *38*, L14812. [CrossRef]
36. Morino, I.; Uchino, O.; Inoue, M.; Yoshida, Y.; Yokota, T.; Wennberg, P.O.; Toon, G.C.; Wunch, D.; Roehl, C.M.; Notholt, J.; et al. Preliminary validation of column-averaged volume mixing ratios of carbon dioxide and methane retrieved from gosat short-wavelength infrared spectra. *Atmos. Meas. Tech.* **2011**, *4*, 1061–1076. [CrossRef]
37. Bergamaschi, P.; Frankenberg, C.; Meirink, J.F.; Krol, M.; Dentener, F.; Wagner, T.; Platt, U.; Kaplan, J.O.; Koerner, S.; Heimann, M.; et al. Satellite chartography of atmospheric methane from sciamachyon board envisat: 2. Evaluation based on inverse model simulations. *J. Geophys. Res. Atmos.* **2007**, *112*, D2. [CrossRef]
38. Bergamaschi, P.; Frankenberg, C.; Meirink, J.F.; Krol, M.; Villani, M.G.; Houweling, S.; Dentener, F.; Dlugokencky, E.J.; Miller, J.B.; Gatti, L.V.; et al. Inverse modeling of global and regional CH_4 emissions using sciamachy satellite retrievals. *J. Geophys. Res. Atmos.* **2009**, *114*, D22. [CrossRef]
39. Bergamaschi, P.; Houweling, S.; Segers, A.; Krol, M.; Frankenberg, C.; Scheepmaker, R.A.; Dlugokencky, E.; Wofsy, S.C.; Kort, E.A.; Sweeney, C.; et al. Atmospheric CH_4 in the first decade of the 21st century: Inverse modeling analysis using sciamachy satellite retrievals and noaa surface measurements. *J. Geophys. Res. Atmos.* **2013**, *118*, 7350–7369. [CrossRef]
40. Houweling, S.; Krol, M.; Bergamaschi, P.; Frankenberg, C.; Dlugokencky, E.J.; Morino, I.; Notholt, J.; Sherlock, V.; Wunch, D.; Beck, V.; et al. A multi-year methane inversion using sciamachy, accounting for systematic errors using tccon measurements. *Atmos. Chem. Phys.* **2014**, *14*, 10961–10962. [CrossRef]
41. Meirink, J.F.; Bergamaschi, P.; Frankenberg, C.; d'Amelio, M.T.S.; Dlugokencky, E.J.; Gatti, L.V.; Houweling, S.; Miller, J.B.; Rockmann, T.; Villani, M.G.; et al. Four-dimensional variational data assimilation for inverse modeling of atmospheric methane emissions: Analysis of sciamachy observations. *J. Geophys. Res. Atmos.* **2008**, *113*, D17. [CrossRef]
42. Cressot, C.; Chevallier, F.; Bousquet, P.; Crevoisier, C.; Dlugokencky, E.J.; Fortems-Cheiney, A.; Frankenberg, C.; Parker, R.; Pison, I.; Scheepmaker, R.A.; et al. On the consistency between global and regional methane emissions inferred from sciamachy, tanso-fts, iasi and surface measurements. *Atmos. Chem. Phys.* **2014**, *14*, 577–592. [CrossRef]
43. Monteil, G.; Houweling, S.; Butz, A.; Guerlet, S.; Schepers, D.; Hasekamp, O.; Frankenberg, C.; Scheepmaker, R.; Aben, I.; Röckmann, T. Comparison of ch4 inversions based on 15 months of gosat and sciamachy observations. *J. Geophys. Res. Atmos.* **2013**, *118*, 11807–11823. [CrossRef]
44. Kort, E.A.; Frankenberg, C.; Costigan, K.R.; Lindenmaier, R.; Dubey, M.K.; Wunch, D. Four corners: The largest us methane anomaly viewed from space. *Geophys. Res. Lett.* **2014**, *41*, 6898–6903. [CrossRef]
45. Buchwitz, M.; Schneising, O.; Reuter, M.; Heymann, J.; Krautwurst, S.; Bovensmann, H.; Burrows, J.P.; Boesch, H.; Parker, R.J.; Somkuti, P.; et al. Satellite-derived methane hotspot emission estimates using a fast data-driven method. *Atmos. Chem. Phys.* **2017**, *17*, 5751–5774. [CrossRef]

46. Crevoisier, C.; Nobileau, D.; Fiore, A.M.; Armante, R.; Chedin, A.; Scott, N.A. Tropospheric methane in the tropics—First year from iasi hyperspectral infrared observations. *Atmos. Chem. Phys.* **2009**, *9*, 6337–6350. [CrossRef]
47. Alexe, M.; Bergamaschi, P.; Segers, A.; Detmers, R.; Butz, A.; Hasekamp, O.; Guerlet, S.; Parker, R.; Boesch, H.; Frankenberg, C.; et al. Inverse modelling of CH_4 emissions for 2010–2011 using different satellite retrieval products from gosat and sciamachy. *Atmos. Chem. Phys.* **2015**, *15*, 113–133. [CrossRef]
48. Buchwitz, M.; Dils, B.; Boesch, H.; Crevoisier, C.; Detmers, R.; Frankenberg, C.; Hasekamp, O.; Hewson, W.; Laeng, A.; Noel, S.; et al. *Product Validation and Intercomparison Report (PVIR)*; Version 4.0, CRDP#3; From ESA Climate Change Initiative (CCI); European Space Agency: Paris, France, 2016; Available online: http://www.esa-ghg-cci.org/?q=node/95 (accessed on 25 August 2017).
49. Hu, H.; Hasekamp, O.; Butz, A.; Galli, A.; Landgraf, J.; Aan de Brugh, J.; Borsdorff, T.; Scheepmaker, R.; Aben, I. The operational methane retrieval algorithm for tropomi. *Atmos. Meas. Tech.* **2016**, *9*, 5423–5440. [CrossRef]
50. Glumb, R.; Davis, G.; Lietzke, C. The tanso-fts-2 instrument for the gosat-2 greenhouse gas monitoring mission. In Proceedings of the 2014 IEEE International Geoscience and Remote Sensing Symposium (IGARSS), Quebec City, QC, Canada, 6 November 2014; pp. 1238–1240.
51. O'Brien, D.M.; Polonsky, I.N.; Utembe, S.R.; Rayner, P.J. Potential of a geostationary geocarb mission to estimate surface emissions of CO_2, CH_4 and CO in a polluted urban environment: Case study shanghai. *Atmos. Meas. Tech.* **2016**, *9*, 4633–4654.
52. Crevoisier, C.; Clerbaux, C.; Guidard, V.; Phulpin, T.; Armante, R.; Barret, B.; Camy-Peyret, C.; Chaboureau, J.P.; Coheur, P.F.; Crépeau, L.; et al. Towards iasi-new generation (iasi-ng): Impact of improved spectral resolution and radiometric noise on the retrieval of thermodynamic, chemistry and climate variables. *Atmos. Meas. Tech.* **2014**, *7*, 4367–4385. [CrossRef]
53. Ehret, G.; Kiemle, C.; Wirth, M.; Amediek, A.; Fix, A.; Houweling, S. Space-borne remote sensing of CO_2, CH_4, and N_2O by integrated path differential absorption Lidar: A sensitivity analysis. *Appl. Phys. B Lasers Opt.* **2008**, *90*, 593–608. [CrossRef]
54. Flamant, P.; Ehret, G.; Millet, B.; Alpers, M. Merlin: A French-German mission addressing methane monitoring by Lidar from space. In Proceedings of the 26th International Laser Radar Conference (ILRC), Porto Heli, Greece, 26–29 June 2012.
55. Kiemle, C.; Quatrevalet, M.; Ehret, G.; Amediek, A.; Fix, A.; Wirth, M. Sensitivity studies for a space-based methane Lidar mission. *Atmos. Meas. Tech.* **2011**, *4*, 2195–2211. [CrossRef]
56. Pierangelo, C.; Millet, B.; Esteve, F.; Alpers, M.; Ehret, G.; Flamant, P.H.; Berthier, S.; Gibert, F.; Chomette, O.; Edouart, D.; et al. Merlin (methane remote sensing Lidar mission): An overview. In Proceedings of the 27th International Laser Radar Conference (ILRC), New York, NY, USA, 5–10 July 2015; EPJ Web of Conferences: Les Ulis, France, 2016; Volume 119.
57. Abshire, J.B.; Riris, H.; Allan, G.R.; Weaver, C.J.; Mao, J.; Sun, X.; Hasselbrack, W.E.; Kawa, S.R.; Biraud, S. Pulsed airborne Lidar measurements of atmospheric CO_2 column absorption. *Tellus B* **2010**, *62*, 770–783. [CrossRef]
58. Amediek, A.; Fix, A.; Wirth, M.; Ehret, G. Development of an opo system at 1.57 μm for integrated path dial measurement of atmospheric carbon dioxide. *Appl. Phys. B* **2008**, *92*, 295–302. [CrossRef]
59. Gibert, F.; Flamant, P.H.; Bruneau, D.; Loth, C. Two-micrometer heterodyne differential absorption Lidar measurements of the atmospheric CO_2 mixing ratio in the boundary layer. *Appl. Opt.* **2006**, *45*, 4448–4458. [CrossRef] [PubMed]
60. Gibert, F.; Flamant, P.H.; Cuesta, J.; Bruneau, D. Vertical 2-μm heterodyne differential absorption Lidar measurements of mean CO_2 mixing ratio in the troposphere. *J. Atmos. Ocean. Technol.* **2008**, *25*, 1477–1497. [CrossRef]
61. Ishii, S.; Mizutani, K.; Fukuoka, H.; Ishikawa, T.; Philippe, B.; Iwai, H.; Aoki, T.; Itabe, T.; Sato, A.; Asai, K. Coherent 2 μm differential absorption and wind Lidar with conductively cooled laser and two-axis scanning device. *Appl. Opt.* **2010**, *49*, 1809–1817. [CrossRef] [PubMed]
62. Koch, G.J.; Barnes, B.W.; Petros, M.; Beyon, J.Y.; Amzajerdian, F.; Yu, J.; Davis, R.E.; Ismail, S.; Vay, S.; Kavaya, M.J.; et al. Coherent differential absorption Lidar measurements of CO_2. *Appl. Opt.* **2004**, *43*, 5092–5099. [CrossRef] [PubMed]

63. Spiers, G.D.; Menzies, R.T.; Jacob, J.; Christensen, L.E.; Phillips, M.W.; Choi, Y.; Browell, E.V. Atmospheric CO_2 measurements with a 2 µm airborne laser absorption spectrometer employing coherent detection. *Appl. Opt.* **2011**, *50*, 2098–2111. [CrossRef] [PubMed]
64. NASA. Ascends: Mission Science Definition and Planning Workshop Report. Available online: https://cce.nasa.gov/ascends (accessed on 24 November 2016).
65. Riris, H.; Numata, K.; Li, S.; Wu, S.; Ramanathan, A.; Dawsey, M.; Mao, J.; Kawa, R.; Abshire, J.B. Airborne measurements of atmospheric methane column abundance using a pulsed integrated-path differential absorption Lidar. *Appl. Opt.* **2012**, *51*, 8296–8305. [CrossRef] [PubMed]
66. Amediek, A.; Ehret, G.; Fix, A.; Wirth, M.; Büdenbender, C.; Quatrevalet, M.; Kiemle, C.; Gerbig, C. Charm-F a new airborne integrated-path differential-absorption Lidar for carbon dioxide and methane observations: Measurement performance and quantification of strong point source emissions. *Appl. Opt.* **2017**, *56*, 5182–5197. [CrossRef]
67. Wirth, M.; Fix, A.; Mahnke, P.; Schwarzer, H.; Schrandt, F.; Ehret, G. The airborne multi-wavelength water vapor differential absorption Lidar wales: System design and performance. *Appl. Phys. B* **2009**, *96*, 201. [CrossRef]
68. Cosentino, A.; D'Ottavi, A.; Sapia, A.; Suetta, E. Spaceborne lasers development for aladin and atlid instruments. In Proceedings of the Geoscience and Remote Sensing Symposium (IGARSS), Munich, Germany, 22–27 July 2012; pp. 5673–5676. [CrossRef]
69. Hunt, W.H.; Winker, D.M.; Vaughan, M.A.; Powell, K.A.; Lucker, P.L.; Weimer, C. Calipso Lidar description and performance assessment. *J. Atmos. Ocean. Technol.* **2009**, *26*, 1214–1228. [CrossRef]
70. Winker, D.M.; Vaughan, M.A.; Omar, A.; Hu, Y.; Powell, K.A.; Liu, Z.; Hunt, W.H.; Young, S.A. Overview of the calipso mission and caliop data processing algorithms. *J. Atmos. Ocean. Technol.* **2009**, *26*, 2310–2323. [CrossRef]
71. Strotkamp, M.; Elsen, F.; Löhring, J.; Traub, M.; Hoffmann, D. Two stage innoslab amplifier for energy scaling from 100 to >500 mj for future Lidar applications. *Appl. Opt.* **2017**, *56*, 2886–2892. [CrossRef] [PubMed]
72. Frankenberg, C.; Meirink, J.F.; Bergamaschi, P.; Goede, A.P.H.; Heimann, M.; Korner, S.; Platt, U.; van Weele, M.; Wagner, T. Satellite chartography of atmospheric methane from sciamachy on board envisat: Analysis of the years 2003 and 2004. *J. Geophys. Res. Atmos.* **2006**, *111*, D07303. [CrossRef]
73. Kuze, A.; Suto, H.; Shiomi, K.; Kawakami, S.; Tanaka, M.; Ueda, Y.; Deguchi, A.; Yoshida, J.; Yamamoto, Y.; Kataoka, F.; et al. Update on gosat tanso-fts performance, operations, and data products after more than 6 years in space. *Atmos. Meas. Tech.* **2016**, *9*, 2445–2461. [CrossRef]
74. Butz, A.; Galli, A.; Hasekamp, O.; Landgraf, J.; Tol, P.; Aben, I. Tropomi aboard sentinel-5 precursor: Prospective performance of CH_4 retrievals for aerosol and cirrus loaded atmospheres. *Remote Sens. Environ.* **2012**, *120*, 267–276. [CrossRef]
75. ESA. Sentinel 5 ESA Webpage. Available online: https://sentinel.esa.int/web/sentinel/missions/sentinel-5;jsessionid=270F0A88C1532B4319622FCF6F80CDA2.jvm2 (accessed on 25 August 2017).
76. Polonsky, I.N.; O'Brien, D.M.; Kumer, J.B.; O'Dell, C.W.; the geo, C.T. Performance of a geostationary mission, geocarb, to measure CO_2, CH_4 and CO column-averaged concentrations. *Atmos. Meas. Tech.* **2014**, *7*, 959–981. [CrossRef]
77. Prather, M.J.; Holmes, C.D.; Hsu, J. Reactive greenhouse gas scenarios: Systematic exploration of uncertainties and the role of atmospheric chemistry. *Geophys. Res. Lett.* **2012**. [CrossRef]
78. Kirschke, S.; Bousquet, P.; Ciais, P.; Saunois, M.; Canadell, J.G.; Dlugokencky, E.J.; Bergamaschi, P.; Bergmann, D.; Blake, D.R.; Bruhwiler, L.; et al. Three decades of global methane sources and sinks. *Nat. Geosci.* **2013**, *6*, 813–823. [CrossRef]
79. Saunois, M.; Jackson, R.B.; Bousquet, P.; Poulter, B.; Canadell, J.G. The growing role of methane in anthropogenic climate change. *Environ. Res. Lett.* **2016**, *11*, 120207. [CrossRef]
80. Chevallier, F.; Broquet, G.; Pierangelo, C.; Crisp, D. Probabilistic global maps of the CO_2 column at daily and monthly scales from sparse satellite measurements. *J. Geophys. Res. Atmos.* **2017**, *122*, 7614–7629. [CrossRef]
81. CAMS. Copernicus Atmosphere Monitoring Service. Available online: http://atmosphere.copernicus.eu/ (accessed on 25 August 2017).
82. Massart, S.; Agusti-Panareda, A.; Aben, I.; Butz, A.; Chevallier, F.; Crevoisier, C.; Engelen, R.; Frankenberg, C.; Hasekamp, O. Assimilation of atmospheric methane products into the macc-ii system: From sciamachy to tanso and iasi. *Atmos. Chem. Phys.* **2014**, *14*, 6139–6158. [CrossRef]

83. Bruhwiler, L.M.; Basu, S.; Bergamaschi, P.; Bousquet, P.; Dlugokencky, E.; Houweling, S.; Ishizawa, M.; Kim, H.S.; Locatelli, R.; Maksyutov, S.; et al. U.S. CH_4 emissions from oil and gas production: Have recent large increases been detected? *J. Geophys. Res. Atmos.* **2017**, *122*, 4070–4083. [CrossRef]
84. Ehret, G.; Kiemle, C. *Requirements Definition for Future Dial Instrument*; ESA Study Report, ESA-CR(P)-4513; European Space Agency: Paris, France, 2003.
85. Loth, C.; Flamant, P.; Bréon, F.M.; Bruneau, D.; Desmet, P.; Pain, T.; Dabas, A.; Prunet, P.; Cariou, J.P. *Future Atmopheric Carbon Dioxide Testing from Space, Observations Techniques and Sensor Concepts for the Observations of CO_2 from Space*; ESA Study Report, ESA-CR(P)-4544; European Space Agency: Paris, France, 2005.
86. Ingmann, P. *A-Scope. Esa Report: Advanced Space Carbon and Climate Observation of Planet Earth, Report for Assessment*; SP-1313/1; ESA/ESTEC: Noordwijk, The Netherlands, 2009.
87. Ehret, G.; Fix, A.; Kiemle, C.; Wirth, A. Space-Borne Monitoring of Methane by Intergrated Parth Differential Absorption Lidar: Perspective of dlr's Charm-SSB Mission. In Proceedings of the 24th International Laser Radar Conference (ILRC), Boulder, Colorado, USA, 23–27 June 2008; pp. 1208–1211.
88. Caron, J.; Durand, Y. Operating wavelengths optimization for a spaceborne Lidar measuring atmospheric CO_2. *Appl. Opt.* **2009**, *48*, 5413–5422. [CrossRef] [PubMed]
89. Fix, A.; Quatrevalet, M.; Witschas, B.; Wirth, M.; Büdenbender, C.; Amediek, A.; Ehret, G. Challenges and solutions for frequency and energy references for spaceborne and airborne integrated path differential absorption Lidars. In Proceedings of the 27th International Laser Radar Conference (ILRC), New York, NY, USA, 5–10 July 2015; EPJ Web of Conferences: Les Ulis, France, 2016; Volume 119, p. 6012.
90. Ehret, G.; Bousquet, P.; Group, M.S.A. *The MERLIN Science Plan*; CNES: Toulouse, France, 2015; Available online: https://files.lsce.ipsl.fr/public.php?service=files&t=1196ccc2dfda89c239d3eb5387da3ca1 (accessed on 25 August 2017).
91. Tellier, Y.; Pierangelo, C.; Wirth, M.; Gibert, F. Averaging bias correction for the future ipda Lidar mission merlin. In Proceedings of the 28th International Laser Radar Conference (ILRC), Bucarest, Romania, 25–30 June 2017.
92. Hungershoefer, K.; Breon, F.M.; Peylin, P.; Chevallier, F.; Rayner, P.; Klonecki, A.; Houweling, S.; Marshall, J. Evaluation of various observing systems for the global monitoring of CO_2 surface fluxes. *Atmos. Chem. Phys.* **2010**, *10*, 10503–10520. [CrossRef]
93. Kaminski, T.; Knorr, W.; Schürmann, G.; Scholze, M.; Rayner, P.J.; Zaehle, S.; Blessing, S.; Dorigo, W.; Gayler, V.; Giering, R.; et al. The bethy/jsbach carbon cycle data assimilation system: Experiences and challenges. *J. Geophys. Res. Biogeosci.* **2013**, *118*, 1414–1426. [CrossRef]

© 2017 by the authors. Licensee MDPI, Basel, Switzerland. This article is an open access article distributed under the terms and conditions of the Creative Commons Attribution (CC BY) license (http://creativecommons.org/licenses/by/4.0/).